Heliyon 11 (2025) e42201

Contents lists available at ScienceDirect

Heliyon

journal homepage: www.cell.com/heliyon

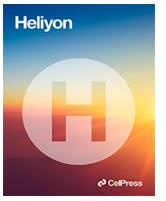

Research article

Identification and functional analysis of energy metabolism and pyroptosis-related genes in diabetic nephropathy

Shan He [1], Jian Ye [1], Yu Wang, Lu yang Xie, Si Yi Liu [*], Qin kai Chen [**]

Department of Nephrology, The First Affiliated Hospital, Jiangxi Medical College, Nanchang University, Nanchang, China

ARTICLE INFO

Keywords:
GEO database
Diabetic nephropathy
Energy metabolism and pyroptosis
Bioinformatics
qRT-PCR

ABSTRACT

Background: Energy metabolism and pyroptosis are integral to the pathogenesis of diabetic nephropathy (DN). However, the precise roles of energy metabolism and pyroptosis in DN development remain unclear. This study aims to elucidate the roles of energy metabolism- and pyroptosis-related differentially expressed genes (EMAPRDEGs) in DN development.

Methods: EMAPRDEGs were identified by querying the GeneCards and Gene Expression Omnibus (GEO) databases. Subsequent analyses included Gene Ontology (GO) and Kyoto Encyclopedia of Genes and Genomes (KEGG) enrichment, Gene Set Enrichment Analysis (GSEA), and Protein-Protein Interaction (PPI) network analysis. Additionally, mRNA-miRNA, mRNA-drug, and mRNA-transcription factor (TF) interaction networks were constructed. Differential expression and receiver operating characteristic (ROC) curve analyses were performed to evaluate the diagnostic potential of EMAPRDEGs. Immune cell infiltration in DN was assessed using the ssGSEA algorithm, and the expression levels of EMAPRDEGs in DN tissues were validated by quantitative real-time PCR (qRT-PCR).

Results: Thirteen EMAPRDEGs were identified, with GO and KEGG analyses indicating their involvement in energy metabolism pathways. GSEA revealed significant enrichment of these genes in biological pathways associated with diabetic nephropathy. PPI network analysis highlighted the central role of these genes within the relevant pathways. Predictive modeling demonstrated interactions between EMAPRDEGs, 69 miRNAs, and 117 TFs. Immune infiltration analysis showed substantial alterations in immune cell populations, with *ADH1B* and *PC* showing a significant correlation with natural killer cells and memory B cells. ROC curve analysis confirmed the diagnostic potential of EMAPRDEGs for diabetic nephropathy. qRT-PCR validated the expression patterns of *CASP1*, *IL-18*, *PDK4*, and *FBP1*, which were consistent with the bioinformatics predictions.

Conclusion: Bioinformatics analysis identified 13 candidate EMAPRDEGs, among which *CASP1*, *IL-18*, *PDK4*, and *FBP1* emerge as potential biomarkers for diabetic nephropathy.

1. Introduction

Diabetic nephropathy (DN) represents a major microvascular complication of diabetes and a leading cause of end-stage renal

* Corresponding author.
** Corresponding author.
E-mail addresses: liusiyi@126.com (S.Y. Liu), timmyclz@163.com (Q. Chen).
[1] Equal contribution authors.

https://doi.org/10.1016/j.heliyon.2025.e42201
Received 12 September 2024; Received in revised form 13 January 2025; Accepted 21 January 2025
Available online 23 January 2025

disease globally, impacting both developing and developed nations [1]. As kidney damage progresses, patients with DN may eventually require chronic renal replacement therapy. Current international guidelines for managing chronic kidney disease (CKD) in type 2 diabetes emphasize controlling hypertension and hyperglycemia, alongside the use of renin-angiotensin system (RAS) blockers, which help reduce urinary protein excretion and inhibit renal fibrosis. However, these treatments often fail to arrest disease progression [2]. Consequently, there is an urgent need for further research into the pathogenesis of DN to facilitate early diagnosis and refine therapeutic strategies. Genetic susceptibility, dysregulation of energy metabolism, and inflammatory processes are all critical factors in the progression of DN.

Energy metabolism plays a pivotal role in the development and progression of DN, with the underlying molecular mechanisms being multifaceted. These include the activation of inflammatory responses, oxidative stress, advanced glycation end products (AGEs), and the production of reactive oxygen species (ROS) [3]. Additionally, metabolic shifts, such as the transition from oxidative phosphorylation to glycolysis, have been observed in podocytes exposed to high glucose levels [4]. This metabolic reprogramming is closely linked to podocyte dedifferentiation and contributes significantly to the pathogenesis of diabetic nephropathy. Beyond the direct effects of hyperglycemia on renal cells, lipid accumulation resulting from lipid metabolism disorders also plays a key role in the onset and progression of DN. Lipid toxicity, arising from lipid accumulation within kidney tissues, induces inflammation and fibrosis, thereby exacerbating the disease process [5]. Pyroptosis, a recently identified form of programmed cell death, is increasingly recognized as a critical mechanism in the pathogenesis of DN [6]. This process is primarily mediated by caspase-1 and gasdermin-D (GSDMD), with the NLRP3/caspase-1/GSDMD pathway serving as a central signaling cascade. Activation of NLRP3 triggers inflammasome formation, leading to the activation of caspase-1, which subsequently cleaves pro-IL-1β and pro-IL-18 into their active forms. The N-terminal domain of GSDMD translocates to the plasma membrane, causing membrane rupture and the release of cellular contents, culminating in pyroptosis [7]. Pyroptosis is a distinct form of programmed cell death (PCD) characterized by its inflammatory nature and specific molecular mechanisms. In contrast to apoptosis, which is a non-inflammatory process leading to cell shrinkage and fragmentation without triggering an immune response [8], pyroptosis culminates in cell lysis and the release of pro-inflammatory cytokines such as IL-1β and IL-18. Unlike necroptosis, another form of inflammatory cell death, pyroptosis is uniquely associated with the Gasdermin family of proteins. These proteins form pores in the cell membrane, resulting in cell swelling and eventual rupture. While necroptosis is regulated by receptor-interacting protein kinases (RIPK1 and RIPK3) and often serves as a compensatory mechanism when apoptosis is impaired, pyroptosis is directly triggered by pathogens or danger signals, establishing it as a critical component of the innate immune response [9]. Recent research suggests that dysregulated energy metabolism pathways can modulate programmed cell death [10,11]. Notably, studies have established a link between energy metabolism and pyroptosis in conditions such as acute kidney injury [12], myocardial injury [13], and cancer [14]. For instance, one study demonstrated that ERRα inhibits pyroptosis in an NLRP3-dependent manner while promoting glycolytic metabolism, thereby conferring cisplatin resistance in endometrial cancer cells [14]. Furthermore, Hao et al. identified that microRNA-17-5p (miR-17-5p) inhibits death receptor-6 (DR-6), thereby supporting the survival of renal tubular epithelial cells during hypoxic/ischemic kidney injury [15], highlighting the close relationship between energy metabolism and pyroptosis in renal tubular cells. However, the gene expression patterns related to energy metabolism and pyroptosis in DN remain unclear. To date, no comprehensive research has specifically examined the interplay between energy metabolism and pyroptosis in DN. This study, therefore, aims to identify key targets associated with energy metabolism and pyroptosis in DN, followed by the prediction of potential therapeutic agents. Further research into the interplay between energy metabolism and pyroptosis could lead to novel therapeutic strategies targeting DN.

In this study, we identified energy metabolism and pyroptosis related differentially expressed genes (EMAPRDEGs), Gene Ontology (GO) and Kyoto Encyclopedia of Genes and Genomes (KEGG) enrichment analysis, as well as Gene Set Enrichment Analysis (GSEA). Differential gene expression and Receiver Operating Characteristic (ROC) analysis were conducted to assess the diagnostic value of these genes. Protein-protein interaction (PPI) networks were constructed using the STRING database to explore interactions between differentially expressed genes (DEGs) in DN and control groups. Additionally, microRNAs (miRNAs) and transcription factors (TFs) targeting EMAPRDEGs were predicted, and gene-drug interaction networks were established. Immune infiltration analysis was performed using single-sample Gene Set Enrichment Analysis (ssGSEA), followed by the examination of EMAPRDEG expression levels in patients with DN and healthy controls. In conclusion, this study investigates the involvement of EMAPRDEGs in DN pathogenesis, offering insights into potential therapeutic avenues.

2. Materials & methods

2.1. Data download

Gene expression data associated with DN was retrieved using the GEOquery package [16], which allowed access to the gene expression database, including the datasets GSE30528 [17]and GSE96804 [18,19]. Dataset GSE30528, derived from Homo sapiens and utilizing the GPL571 platform, consists of 22 samples, with 9 samples from patients with DN (group: DN) and 13 from healthy controls (group: Control). Dataset GSE96804, sourced from the GPL17586 platform and also originating from Homo sapiens, includes 61 samples, comprising 41 samples from patients with DN (group: DN) and 20 from healthy controls (group: Control). Both datasets were included in this analysis. To address potential batch effects for data sets GSE30528 and GSE96804, the R package sva (Version 3.50.0) [20] was utilized for batch effect removal before conducting differential expression analysis. The Surrogate Variable Analysis (SVA) method adjusts for experimental batches or other biological factors that might introduce systematic biases, thereby optimizing the consistency of sample expression patterns. This step ensures that the results are not confounded by batch effects, enhancing the reliability of subsequent analyses. Detailed information about the datasets is presented in Table 1. Following batch effect correction,

the two datasets were combined, resulting in a unified dataset comprising 50 DN samples and 33 control samples.

To identify genes related to energy metabolism and pyroptosis (EMAPRGs), a comprehensive search was performed using the terms "Energy metabolism" and "Pyroptosis" in the GeneCards database [21] (https://www.genecards.org/). Filtering with the criteria "Protein Coding" and "Score >2," a total of 564 energy metabolism-related genes (EMRGs) and 59 pyroptosis-related genes (PRGs) were identified. Additionally, 629 EMRGs [22–25]and 52 PRGs [26] were identified from the published literature. The initial genes related to energy metabolism identified were intersected and deduplicated, resulting in 105 EMRGs, while the initial genes related to pyroptosis were merged and deduplicated to obtain 26 PRGs. The integration of these sets revealed 131 EMAPRGs.

2.2. Analysis of differentially expressed genes

Differential expression analysis of transcriptome data from the DN datasets was conducted using the limma tool. Genes with a $|\log FC| > 0.15$ and P-value <0.05 were classified as DEGs. Among these, genes with logFC >0.15 and P-value <0.05 were categorized as up-regulated, while those with logFC < - 0.15 and P-value <0.05 were classified as down-regulated.

To identify EMAPRDEGs, the intersection of all DEGs from the DN datasets and EMAPRGs was obtained and visualized using a Venn diagram. The overlapping genes were designated as EMAPRDEGs for further analysis. The results of the differential expression analysis were visualized through volcano plots generated with the ggplot2 package in R. Heatmaps of EMAPRDEGs were constructed using the pheatmap package (Version 1.0.12) in R.

2.3. Functional and pathway enrichment analysis

GO analysis was performed across three main domains: Molecular Function (MF), Cellular Component (CC), and Biological Process (BP) [27]. KEGG [28] a widely used database, provides comprehensive information on genomes, biological processes, diseases, and medications. The R package clusterProfiler [29] was employed to perform GO and KEGG analyses on the list of differentially expressed genes.

Statistical significance was considered for adjusted P-values (P.adj) < 0.05 and false discovery rate (FDR) values (Q.value) < 0.25, with P-values corrected using the Benjamini-Hochberg (BH) method to minimize false positives.

2.4. Gene set enrichment analysis (GSEA)

GSEA [30] a statistical method for evaluating the enrichment of predefined gene sets in a ranked list of genes, was applied to assess the relationship between gene sets and specific phenotypes. In this study, genes from the DN datasets were ranked based on their logFC values, and GSEA was performed on all differentially expressed genes using the ClusterProfiler package. The analysis included a seed value of 2022, 5000 permutations, and a gene set size range of 10–500 genes. The "c2.all.v2022.1.Hs" gene set from the MSigDB database [31] was used. Statistical significance was defined by adjusted P-values (P.adj) < 0.05 and FDR values (Q.value) < 0.25, with P-values corrected using the BH method to control for false positives.

2.5. Differential expression analysis and ROC analysis of EMAPRDEGs

The Mann-Whitney *U* test, also known as the Wilcoxon rank-sum test, was employed to evaluate the differences in EMAPRDEG expression between the disease and control groups in the DN datasets. Group comparison maps were created using the ggplot2 package in R, providing a visual representation of the differential expression analysis results.

For diagnostic evaluation of the EMAPRDEGs, the receiver operating characteristic (ROC) curve [32] was constructed to depict the relationship between sensitivity and specificity. The pROC package in R was used to generate the ROC curve for the EMAPRDEGs and to compute the area under the curve (AUC) value, which serves as a measure of diagnostic accuracy in DN. The AUC value ranges from 0.5 to 1, with a higher AUC indicating better diagnostic performance. Specifically, an AUC between 0.5 and 0.7 suggests relatively low

Table 1
GEO Dataset Information list.

	GSE30528	GSE96804
Platform	GPL571	GPL17586
Experiment type	Expression profiling by array	Expression profiling by array
Species	Homo sapiens	Homo sapiens
Tissue	glomeruli	glomeruli
Samples in Control group	Control (13)	Control(20)
Samples in Disease group	DN(9)	DN(41)
Reference	Transcriptome analysis of human diabetic kidney disease.	Dissection of Glomerular Transcriptional Profile in Patients With Diabetic Nephropathy: SRGAP2a Protects Podocyte Structure and Function. Identification of Transcription Regulatory Relationships in Diabetic Nephropathy.

DN,Diabetic nephropathy.

diagnostic accuracy, an AUC between 0.7 and 0.9 signifies moderate accuracy, and an AUC exceeding 0.9 reflects high diagnostic accuracy.

2.6. Protein-protein interaction network (PPI) and functional similarity analysis

The STRING database [33], a comprehensive resource for protein interaction analysis, was utilized in this study with a focus on human species interactions. To ensure the reliability of the results, a stringent filter was applied, setting a minimum interaction score of 0.150. The filtered interaction data were then used to construct a PPI network, which was visualized using Cytoscape [34] software to provide an intuitive representation of the complex interaction landscape.

GO annotation provides an empirical framework for assessing functional similarities across genes and genomes, serving as a vital tool in bioinformatics. The GOSemSim package [35] was employed to evaluate the semantic similarity of EMAPRDEGs, calculating a composite score based on the geometric mean of three GO domains: BP, CC, and MF. The ggplot tool was then used to visualize the results of this functional similarity analysis.

The GeneMANIA [36] database facilitates hypothesis generation regarding gene functions, allowing for the analysis and prioritization of genes based on their interactions. It also supports the prediction of gene functions by identifying genes with similar profiles to a query gene. In this study, genes with similar functions to the hub genes were predicted using GeneMANIA, and the resulting interaction network was downloaded. The figure displays differentially expressed genes in the inner circle, while the outer circle represents genes with analogous functions. The color of the connecting lines indicates the functional relationships between these genes.

2.7. mRNA-miRNA, mRNA-Drug and mRNA-TF interaction network

The Starbase 3.0 database [37], which contains extensive interaction data on miRNA-ncRNA, miRNA-mRNA, miRNA-RNA, and RNA-RNA relationships, was utilized to identify miRNA targets based on experimental data from CLIP-seq and degradome. A filtering criterion of pancancerNum >10 was applied to select mRNA-miRNA interactions. Cytoscape software was then employed to visualize the mRNA-miRNA interaction network.

The Comparative Toxicogenomics Database (CTD) [38] was leveraged to predict both primary and secondary drug targets for the EMAPRDEGs. To explore the interactions between these genes and drugs, the "ReferenceCount" > 4 criterion was applied to select significant mRNA-drug interactions. Cytoscape was used to visualize and integrate these mRNA-drug interaction data, generating a comprehensive network.

TFs that interact with the EMAPRDEGs were identified using the CHIPBase database (version 3.0) [37]. The mRNA-TF interaction pairs were filtered based on the sum of "Num. samples (upstream)" and "Num. samples (downstream)" being greater than 8. Cytoscape was then employed to generate a visual representation of the mRNA-TF interaction network, illustrating the intricate connections between the mRNAs and their associated transcription factors.

2.8. Single-sample gene-set enrichment analysis (ssGSEA)

The ssGSEA [39] methodology was applied to calculate the relative concentration of immune cell infiltrates. Using the ssGSEA algorithm from the GSVA package in R, enrichment scores were computed to quantify the infiltration of various immune cell types across the samples. Boxplots were generated to depict the differences in immune cell infiltration among disease and control groups in the DN datasets. The gene expression matrix from the DN datasets was then analyzed to examine correlations between immune cell profiles and disease status.

Additionally, the association between immune cells and EMAPRDEGs was analyzed, with the R package 'ggplot2' utilized to visualize the correlation data.

2.9. Quantitative real-time PCR (qRT-PCR)

Between July and August 2024, a total of nine whole-blood specimens were collected from the First Affiliated Hospital of Nanchang University, consisting of six samples from patients with DN and three from healthy controls, all aged between 30 and 65 years. Informed consent was obtained from all participants, and the study received ethical approval from the Institutional Ethics Committee (Ethical number: (2024) CDYFYYLK (07–026)). A volume of 3–5 mL of whole blood was drawn from each participant into EDTA-containing tubes for white blood cell (WBC) enrichment. Blood samples from patients with DN were collected prior to any treatment. Total RNA was extracted from the enriched samples. Reverse transcription was performed using the Servicebio® RT First Strand cDNA Synthesis Kit (Servicebio, Wuhan, China), according to the manufacturer's protocol. For quantitative PCR (qPCR), the 2 × SYBR Green qPCR Master Mix (None ROX) from Servicebio was employed, following the provided guidelines. The thermocycling conditions were as follows: an initial denaturation at 95 °C for 5 min, followed by 40 cycles of denaturation at 95 °C for 10 s and annealing/extension at 60 °C for 30 s. ACTIN was used as the reference gene for data normalization, and gene expression was calculated using the $2^{-\Delta\Delta Ct}$ method. The primers used for the experiment are listed in Table 8.

2.10. Statistical analysis

Data processing and analysis were conducted using R software (Version 4.2.2). For comparisons of continuous variables between two groups, the independent Student's t-test was applied when the data followed a normal distribution. In cases where the data did not exhibit a normal distribution, the Mann-Whitney *U* test (also known as the Wilcoxon rank-sum test) was employed to assess differences between the groups. The Kruskal-Wallis test was utilized for comparisons involving more than two groups.

Categorical variables between two groups were analyzed using either the Chi-square test or Fisher's exact test, depending on the dataset's characteristics. Spearman's correlation analysis was applied to explore the relationships among variables. All P-values were calculated as two-tailed, and a P-value of less than 0.05 was considered statistically significant.

3. Results

3.1. Technology Roadmap

Depicted in Fig. 1.

3.2. Data set correction

Batch correction for the DN datasets was initially performed using the R package sva, resulting in corrected datasets. To evaluate the effectiveness of the correction, a comparative analysis was conducted on the datasets before and after batch correction. This included generating density boxplots and principal component analysis (PCA) plots (Fig. 2A–D), which demonstrated a significant reduction in batch effects post-correction, as evident from the improved clustering and distribution in the corrected datasets.

3.3. Analysis of differentially expressed genes

To identify DEGs across various DN groups, differential expression analysis was carried out using the limma package in R. A total of 1308 genes were identified as DEGs based on the criteria of $|\log FC| > 0.15$ and P-value <0.05. Specifically, 608 genes were upregulated ($\log FC > 0.15$) and 700 genes were downregulated ($\log FC < -0.15$) between the DN and control groups, as revealed through variance analysis and visualized in the volcano plot (Fig. 3A). To identify EMAPRDEGs, the DEG dataset was intersected with the EMAPRGs. Thirteen genes were identified as EMAPRDEGs for further analysis (Table 2), and their overlap was illustrated in a Venn diagram (Fig. 3B).

A heatmap depicting the differential expression of the 13 EMAPRDEGs between the DN and control groups is shown in Fig. 3C, where gene names are arranged in descending order of log FC.

To investigate the chromosomal location of the 13 EMAPRDEGs, annotations were made using the RCircos package (Fig. 3D). These

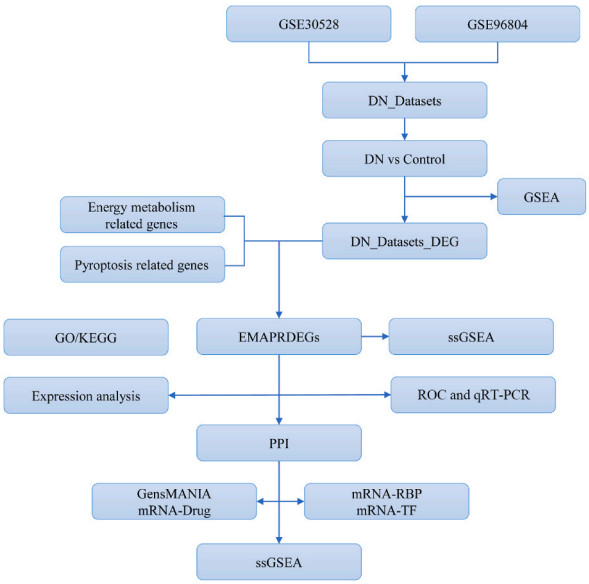

Fig. 1. Technology Roadmap DN, Diabetic nephropathy. DEG, Differentially expressed genes. EMAPRDEGs, Energy metabolism and pyroptosis related differentially expressed genes. GSEA, Gene set enrichment analysis. GO, Gene ontology. KEGG, Kyoto encyclopedia of genes and genomes. ssGSEA, single-sample gene-set enrichment Analysis. ROC, Receiver operating characteristic curve. PPI, Protein-protein interaction network. TF, Transcription factors. RBP, RNA binding protein. qRT-PCR, Quantitative real-time PCR.

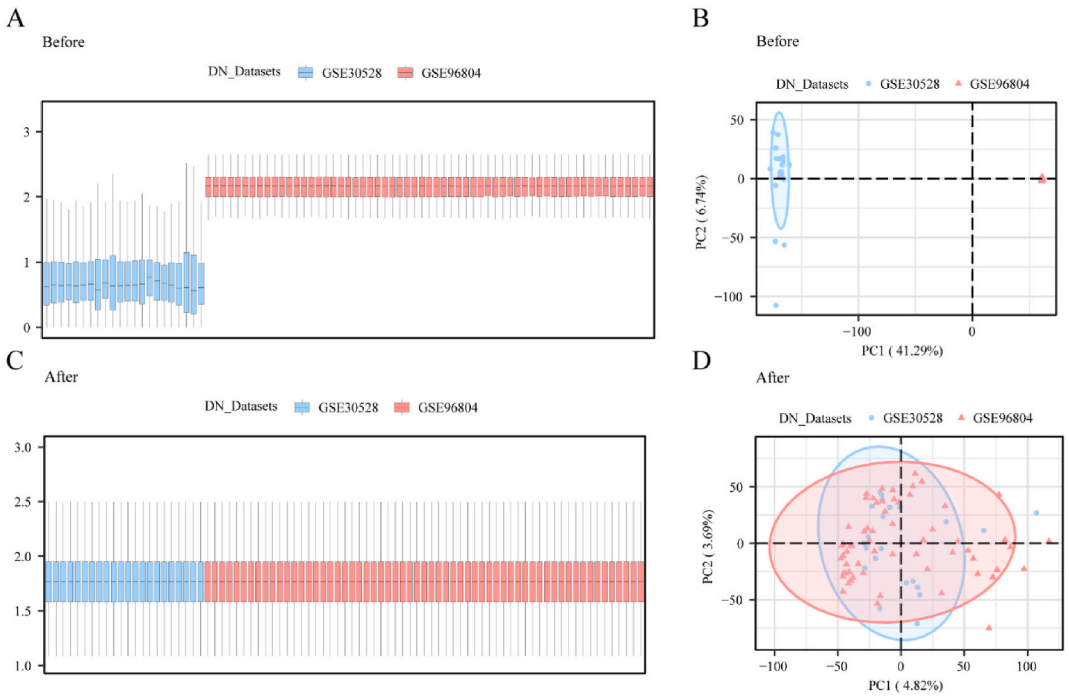

Fig. 2. Dataset correction A. boxplot of the DN Datasets dataset before correction. Shows the distribution of data before batching. In the boxplot, the light blue box represents data set GSE30528, while the light red box represents data set GSE96804. B. PCA plot of DN Datasets before correction. Shows the results of principal component analysis (PCA) of the sample before batch removal, with the first two principal components (PC1 and PC2) represented on the X and Y axes, respectively. C. boxplot plot of the corrected DN Datasets dataset. shows the distribution of the data set after batching. D. PCA plot of the corrected DN Datasets dataset. DN, Diabetic nephropathy. Shows the PCA results of a sample after batch removal. The Diabetic nephropathy (DN) dataset GSE30528 is in light blue, and the Diabetic nephropathy (DN) dataset GSE96804 is in light red.

EMAPRDEGs were predominantly located on chromosomes 1, 4, 6, 7, 9, 10, 11, and 15, with chromosome 11 showing the highest concentration of EMAPRDEGs (four genes). The close proximity of these genes on chromosome 11 suggests a robust genomic correlation among them.

3.4. Functional and pathway enrichment analysis

To elucidate the underlying biological mechanisms associated with the 13 EMAPRDEGs (*CASP3*, *ADH1B*, *TALDO1*, *PDK4*, *SDHB*, *PC*, *CASP1*, *FBP1*, *ACOT13*, *IL18*, *PCK1*, *IQGAP1*, *PFKFB3*), GO analysis was conducted, focusing on MFs, BPs, and CCs (Table 3). The analysis revealed that these EMAPRDEGs were primarily enriched in BPs such as hexose metabolic processes, monosaccharide metabolic processes, pyruvate metabolism, glucose metabolic processes, and cellular carbohydrate metabolic processes. This suggests a potential role of these genes in regulating energy production and metabolism. Regarding CC, enrichment was observed in the mitochondrial matrix, which implicates these genes in mitochondrial functions, particularly in the respiratory chain and energy production. The mitochondria's role in energy metabolism and apoptosis is well-documented, further supporting the involvement of these genes in regulating cellular energy homeostasis and apoptosis. In terms of MF, the enriched terms included carbohydrate phosphatase activity, sugar-phosphatase activity, monosaccharide binding, carboxylic acid binding, and carbohydrate binding. These functions are closely related to sugar phosphorylation and enzyme activity, which are essential for regulating substrate flux through various metabolic pathways. Subsequently, KEGG pathway enrichment analysis was performed on the 13 EMAPRDEGs (Table 3). The results highlighted significant enrichment in key metabolic pathways, including carbon metabolism, the citrate cycle (TCA cycle), glycolysis/gluconeogenesis, and the AMPK signaling pathway, all of which are central to cellular energy production. To visually represent these findings, bar charts (Fig. 4A) and bubble charts (Fig. 4B) were constructed for the GO and KEGG enrichment analyses. Additionally, network diagrams for biological processes (BP, Fig. 4C), molecular functions (MF, Fig. 4D), cellular components (CC, Fig. 4E), and KEGG pathways (Fig. 4F) were generated. These network diagrams illustrate the connections between the EMAPRDEGs and their respective annotations. The size of each node in the diagrams corresponds to the number of molecules within each entry, with larger nodes indicating a higher quantity of associated molecules.

3.5. GSEA enrichment analysis

GSEA was conducted to explore the correlation between gene expression and relevant biological processes, cellular components,

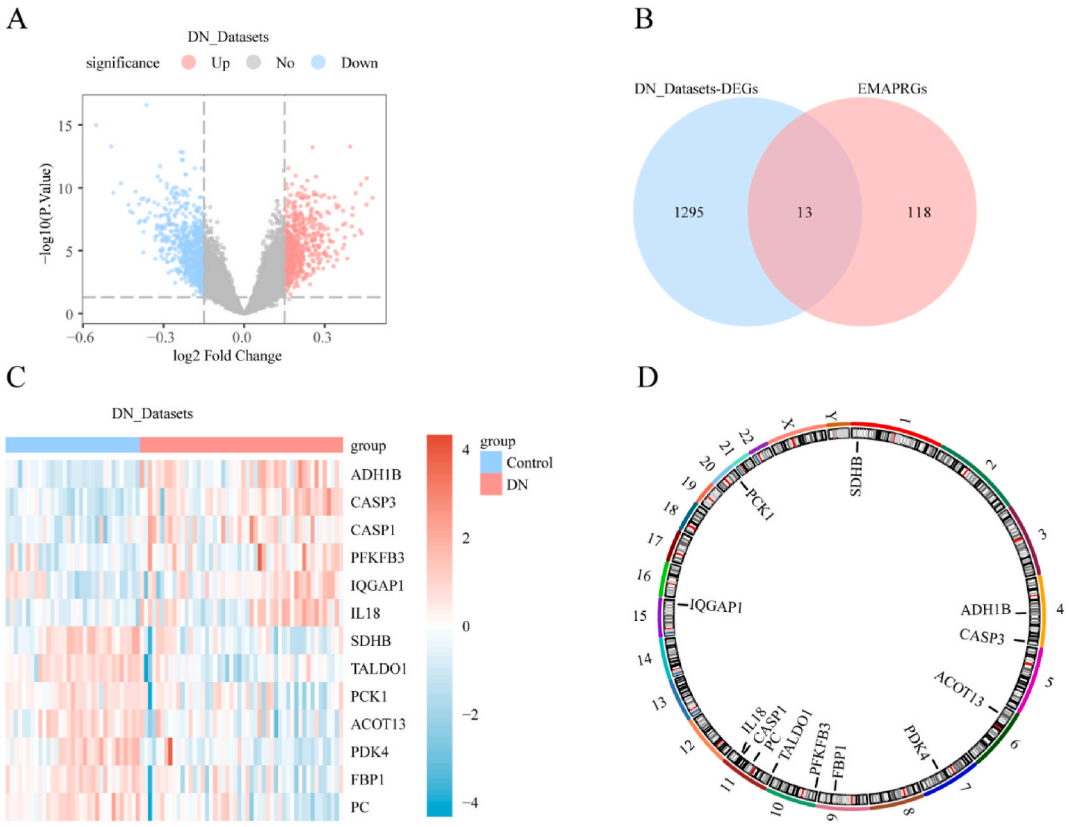

Fig. 3. Analysis of differentially expressed genes A. Volcano plot of differential analysis results between DN and Control groups in the DN Datasets dataset. B. Venn diagram of differential genes in DN Datasets dataset. C. Differential expression heatmap of EMAPRDEGs in DN Datasets dataset. D. Chromosomal localization map. DN, Diabetic nephropathy. DEGs, Differentially expressed genes. EMAPRDEGs, Energy metabolism and pyroptosis related differentially expressed genes. Light red is diabetic nephropathy (DN) group, light blue is Control (Control) group. In the heat map, red represents high expression and blue represents low expression.ADH1B-Alcohol Dehydrogenase 1B; CASP3-Caspase 3; CASP1-Caspase 1; PFKFB3-6-Phosphofructo-2-Kinase/Fructose-2,6-Biphosphatase 3; IQGAP1-IQ Motif Containing GTPase Activating Protein 1; IL18-Interleukin 18; SDHB-Succinate Dehydrogenase Complex Iron Sulfur Subunit B; TALDO1-ransaldolase 1; PCK1-Phosphoenolpyruvate Carboxykinase 1; ACOT13-Acyl-CoA Thioesterase 13; PDK4-Pyruvate Dehydrogenase Kinase 4; FBP1-Fructose-Bisphosphatase 1; PC-Pyruvate Carboxylase.

Table 2
EMAPRDEGs in DN datasets.

	logFC	AveExpr	t	P.Value	adj.P.Val	B	group
ADH1B	0.367566	1.887138	6.427951	6.67E-09	5.94E-07	10.13912	up
CASP3	0.235233	1.968116	7.635668	2.69E-11	1.41E-08	15.43041	up
CASP1	0.205021	1.840216	4.795175	6.65E-06	9.50E-05	3.552582	up
PFKFB3	0.176863	1.769025	3.248742	0.001648	0.006893	−1.59571	up
IQGAP1	0.163056	2.067314	3.633964	0.000471	0.002566	−0.4441	up
IL18	0.158416	1.76176	4.109908	8.93E-05	0.000697	1.105967	up
SDHB	−0.1729	2.020003	−5.18056	1.41E-06	2.94E-05	5.023465	down
TALDO1	−0.18622	2.171838	−5.59438	2.52E-07	8.25E-06	6.666832	down
PCK1	−0.1926	2.201158	−3.88242	0.000201	0.001317	0.348477	down
ACOT13	−0.19821	1.935578	−4.48063	2.25E-05	0.000242	2.400666	down
PDK4	−0.20604	1.868367	−5.52267	3.41E-07	1.01E-05	6.377741	down
FBP1	−0.21668	2.191973	−4.4887	2.18E-05	0.000236	2.429621	down
PC	−0.21989	2.112074	−5.0895	2.05E-06	3.91E-05	4.670416	down

DN, Diabetic nephropathy. EMAPRDEGs, Energy metabolism and Pyroptosis related differentially expressed genes.

and molecular functions in the DN datasets. Enrichment analysis was conducted to identify pathways with significant statistical enrichment (P. adj <0.05 and FDR value [Q. value] < 0.25). The top four pathways exhibiting the highest NES were selected for presentation. These results were visualized through a mountain plot (Fig. 5A) and a GSEA classical enrichment map (Fig. 5B–E). The analysis revealed substantial gene enrichment in processes such as collagen fibril assembly and the formation of other multimeric

Table 3
GO/KEGG enrichment analysis results.

ONTOLOGY	ID	Description	GeneRatio	BgRatio	pvalue	p.adjust	qvalue
BP	GO:0019318	hexose metabolic process	5/12	242/18800	2.4951E-07	8.1852E-05	4.0358E-05
BP	GO:0005996	monosaccharide metabolic process	5/12	261/18800	3.6304E-07	8.1852E-05	4.0358E-05
BP	GO:0006090	pyruvate metabolic process	4/12	106/18800	4.5642E-07	8.1852E-05	4.0358E-05
BP	GO:0006006	glucose metabolic process	4/12	201/18800	5.8699E-06	0.00078951	0.00038927
BP	GO:0044262	cellular carbohydrate metabolic process	4/12	287/18800	2.3905E-05	0.00142899	0.00070457
CC	GO:0005759	mitochondrial matrix	3/12	473/19594	0.00261407	0.09149242	0.08254955
MF	GO:0019203	carbohydrate phosphatase activity	2/12	10/18410	1.7476E-05	0.00074273	0.0004323
MF	GO:0050308	sugar-phosphatase activity	2/12	10/18410	1.7476E-05	0.00074273	0.0004323
MF	GO:0048029	monosaccharide binding	2/12	71/18410	0.00094398	0.02674614	0.01556741
MF	GO:0031406	carboxylic acid binding	2/12	173/18410	0.00544685	0.05507475	0.03205589
MF	GO:0030246	carbohydrate binding	2/12	270/18410	0.01283648	0.05507475	0.03205589
KEGG	hsa01200	Carbon metabolism	4/11	115/8164	1.1426E-05	0.00033135	0.00021048
KEGG	hsa00020	Citrate cycle (TCA cycle)	3/11	30/8164	7.2441E-06	0.00033135	0.00021048
KEGG	hsa00620	Pyruvate metabolism	3/11	47/8164	2.8572E-05	0.00055238	0.00035088
KEGG	hsa00010	Glycolysis/Gluconeogenesis	3/11	67/8164	8.3175E-05	0.00120604	0.00076609
KEGG	hsa04152	AMPK signaling pathway	3/11	121/8164	0.00048045	0.00557325	0.00354018

GO, Gene ontology; BP, Biological process; CC, Cellular component; MF, Molecular function; KEGG, Kyoto encyclopedia of genes and genomes.

structures, as illustrated in Fig. 5B. Furthermore, pathways related to the inflammatory response mechanism (Fig. 5C), MET-mediated motility promotion (Fig. 5D), and the regulation of Wnt/β-catenin signaling by small molecule compounds (Fig. 5E) were also identified (Table 4).

3.6. Differential expression analysis and ROC analysis of EMAPRDEGs

The expression profiles of 13 EMAPRDEGs (*CASP3*, *ADH1B*, *TALDO1*, *PDK4*, *SDHB*, *PC*, *CASP1*, *FBP1*, *ACOT13*, *IL18*, *PCK1*, *IQGAP1*, *PFKFB3*) were compared between the DN and control groups in the DN datasets. The results of this differential expression analysis are displayed in the group comparison plot (Fig. 6A). These findings highlighted significant differences in the expression of the 13 EMAPRDEGs between DN and control groups ($P < 0.05$). Subsequently, ROC curves were constructed using the expression levels of these genes in both the DN and control groups (Fig. 6B–F). The analysis demonstrated that *CASP3* exhibited a high diagnostic accuracy for DN, with an AUC of 0.918 (Fig. 6B). Other genes, including *ADH1B* (AUC = 0.851), *TALDO1* (AUC = 0.875), *PDK4* (AUC = 0.853, Fig. 6C), *SDHB* (AUC = 0.798), *PC* (AUC = 0.805), *CASP1* (AUC = 0.772, Fig. 6D), *FBP1* (AUC = 0.759), *ACOT13* (AUC = 0.772), *IL18* (AUC = 0.715, Fig. 6E), *PCK1* (AUC = 0.728), *IQGAP1* (AUC = 0.729, Fig. 6F), and *PFKFB3* (AUC = 0.707), also displayed varying degrees of diagnostic accuracy in identifying DN.

3.7. PPI network and functional similarity analysis

The STRING database was employed to analyze PPI of the 13 EMAPRDEGs (*CASP3*, *ADH1B*, *TALDO1*, *PDK4*, *SDHB*, *PC*, *CASP1*, *FBP1*, *ACOT13*, *IL18*, *PCK1*, *IQGAP1*, *PFKFB3*). Following the filtration of EMAPRDEGs exhibiting interactions with other nodes, a set of 13 EMAPRDEGs was identified for further analysis, and a PPI network was constructed and visualized using Cytoscape software (Fig. 7A).

Subsequently, functional similarity analysis of the 13 EMAPRDEGs in the PPI network was performed. The R program GOSemSim was utilized to compute the semantic similarity among the gene products and associated gene clusters, which involved calculating GO terms and sets. The functional similarity results for key genes were presented through boxplots (Fig. 7B). The analysis revealed that FBP1 exhibited the highest degree of functional similarity with other major genes within the network.

Additionally, the GeneMANIA database was used to explore the correlations between the 13 EMAPRDEGs and other genes (Fig. 7C). The findings indicated that these 13 EMAPRDEGs primarily exhibited co-expression and physical interactions with other genes, further highlighting their involvement in interconnected biological processes.

3.8. mRNA-miRNA, mRNA-Drug, mRNA-TF interaction network

The Starbase 3.0 database was utilized to predict miRNAs interacting with the 13 EMAPRDEGs (*CASP3*, *ADH1B*, *TALDO1*, *PDK4*, *SDHB*, *PC*, *CASP1*, *FBP1*, *ACOT13*, *IL18*, *PCK1*, *IQGAP1*, *PFKFB3*). Filtering was performed using the criterion of pancancerNum >10, and the results were visualized with Cytoscape software (Fig. 8A). The analysis revealed an mRNA-miRNA interaction network comprising 6 mRNAs (*CASP3*, *IQGAP1*, *PC*, *PDK4*, *PFKFB3*, *SDHB*) and 55 miRNAs, representing 69 distinct interactions between mRNA and miRNA. The precise interactions are detailed in Table 5.

Additionally, the CTD database was employed to predict potential drugs or small molecule compounds interacting with the 13 EMAPRDEGs. mRNA-drug interaction pairs were filtered with the criterion of "reference count" > 4, and the results were visualized using Cytoscape software (Fig. 8B). This analysis identified 6 mRNAs (*ADH1B*, *CASP3*, *FBP1*, *IL18*, *PC*, *PFKFB3*) and 51 different drug molecules, resulting in 53 unique mRNA-drug interactions. Detailed interaction data are provided in Table 6.

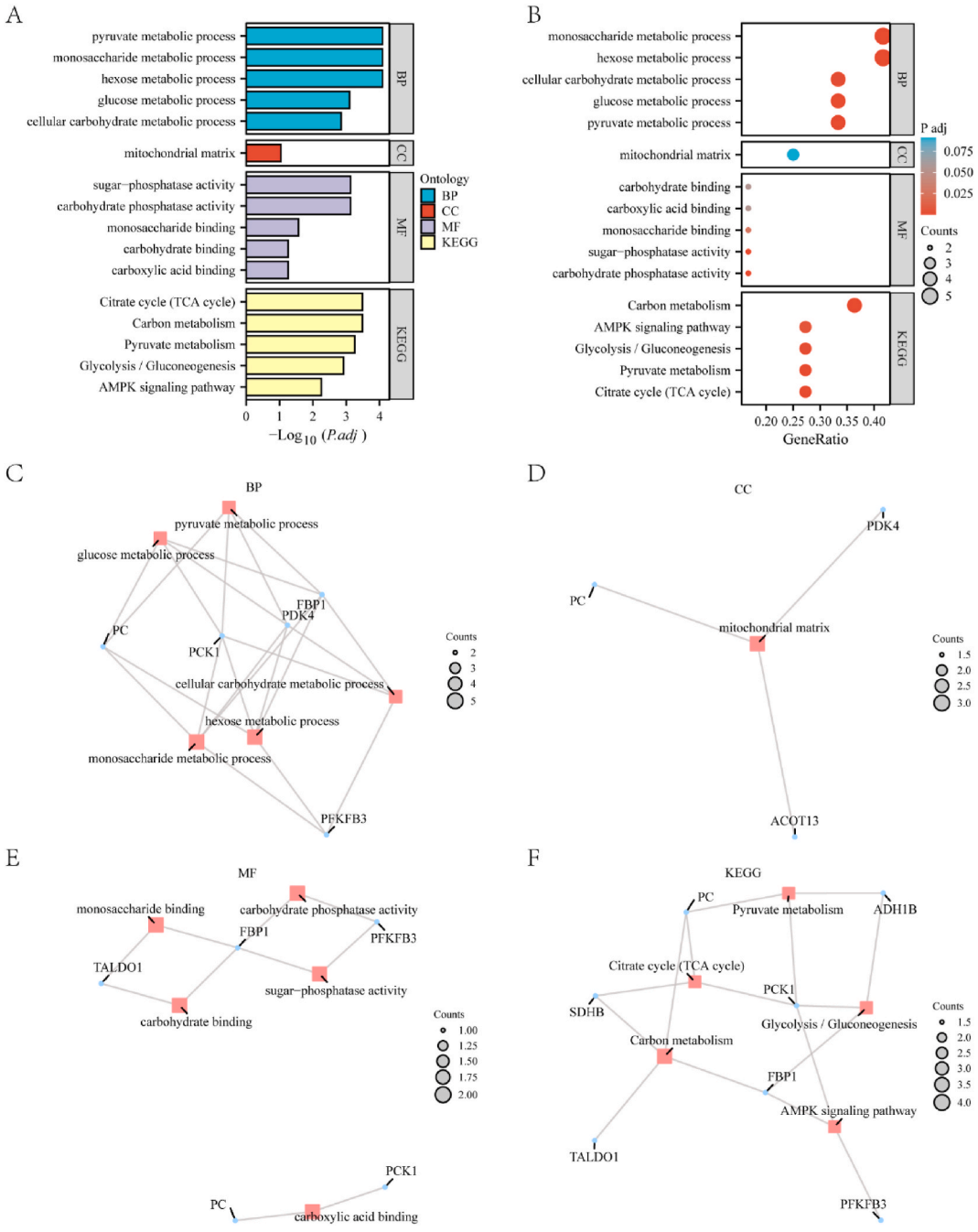

Fig. 4. Functional enrichment analysis (GO) and pathway enrichment (KEGG) analysis A. Bar graph of GO and KEGG enrichment analysis results of EMAPRDEGs. B. Bubble plot of GO and KEGG enrichment analysis results of EMAPRDEGs. The ordinate is the GO terms and KEGG terms. The bubble map shows the importance and number of genes of 13 EMAPRDEGs enriched entries in the GO (Gene Ontology) and KEGG (Kyoto Genome Encyclopedia) categories. Each bubble represents a specific biological process (BP), cell component (CC), molecular function (MF), or pathway (KEGG), and its size and color indicate the number and statistical significance of the genes involved, respectively. C-E. Network diagram of GO enrichment analysis results of EMAPRDEGs (C: BP, D: CC, E: MF). F. Network diagram of KEGG enrichment analysis results of EMAPRDEGs. In the network diagram (C–F), red dots represent specific pathways and blue dots represent specific genes. GO, Gene ontology. KEGG, Kyoto encyclopedia of genes and genomes. BP, Biological process. CC, Cellular component. MF, Molecular function. EMAPRDEGs, Energy metabolism and pyroptosis related differentially expressed genes. The screening criteria for GO/KEGG enrichment items were p. Adj <0.05 and FDR value (q. value) < 0.25, and the p value correction method was Benjamini-Hochberg (BH).

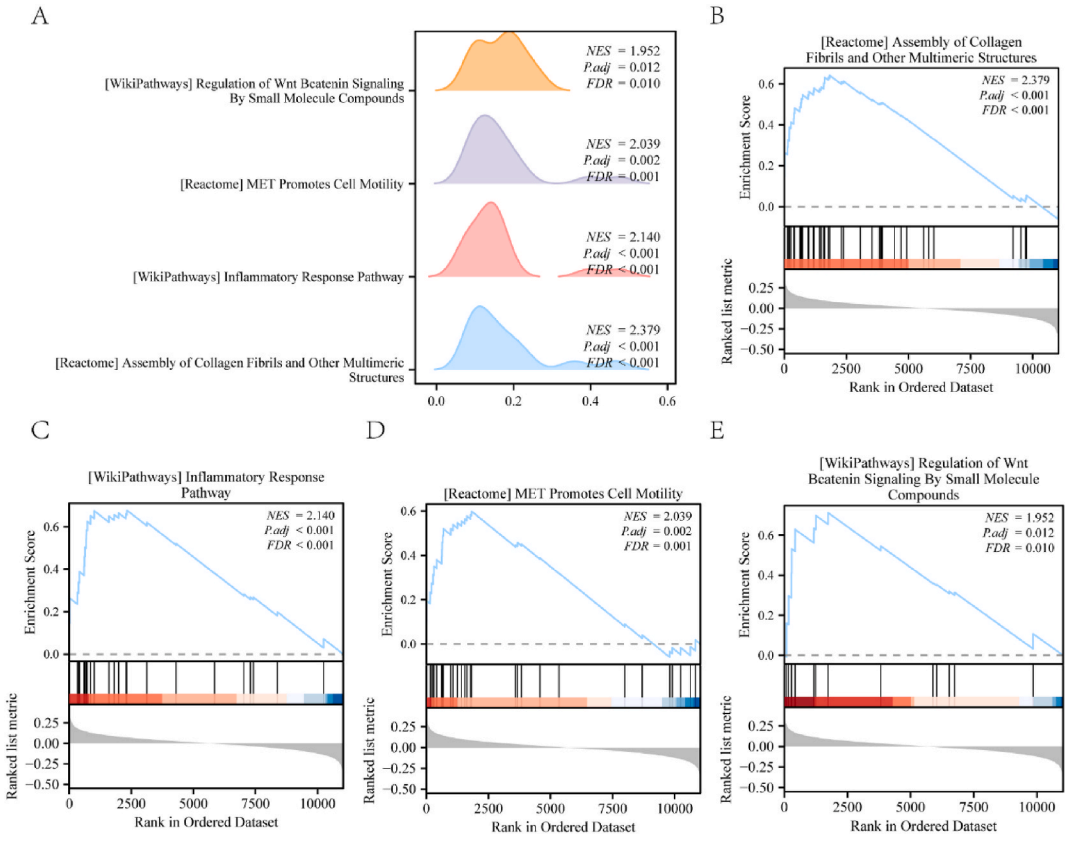

Fig. 5. GSEA of DN Datasets dataset A. GSEA of DN Datasets dataset mountain map of main four biological functions. B-E. Genes in DN Datasets were significantly enriched in Assembly of collagen fibrils and other multimeric structures (B), Inflammatory response pathway (C), MET promotes motility (D), Regulation of Wnt/β-catenin signaling by small molecule compounds (E), GSEA, Gene set enrichment analysis. DN, Diabetic nephropathy. The screening criteria of gene set enrichment analysis (GSEA) were p. Adj< 0.05 and FDR value (q value) < 0.25, and the p value correction method was Benjamini-Hochberg (BH).

To explore the interactions between the 13 EMAPRDEGs and transcription factors (TFs), a search in the CHIPBase database (version 3.0) was conducted. The screening criterion for mRNA-TF interactions was a combined count of upstream and downstream samples exceeding 8. The mRNA-TF interaction network was visualized using Cytoscape (Fig. 8C). This network revealed 12 mRNAs (*CASP3*, *ADH1B*, *TALDO1*, *PDK4*, *SDHB*, *PC*, *CASP1*, *FBP1*, *ACOT13*, *IL18*, *IQGAP1*, *PFKFB3*) and 45 TFs, with 117 documented interactions between mRNAs and TFs, as detailed in Table 7.

3.9. Single-sample gene set enrichment analysis (ssGSEA)

The ssGSEA algorithm was employed to assess variations in immune cell infiltration between the DN and control groups (DN/Control) across 28 distinct immune cell types. The results were visualized using a group comparison plot (Fig. 9A). Statistically significant differences ($P < 0.05$) were observed in the infiltration levels of 15 immune cell types between the DN and control groups. A correlation analysis was performed to compute the relationships between the levels of these 15 immune cells across the disease and control samples, with the results depicted in Fig. 9B. In the DN dataset, the strongest positive correlation ($r = 0.82$) was observed between regulatory T cells and memory B cells, whereas the most prominent negative correlation ($r = -0.58$) was identified between immature dendritic cells and immature B cells.

Further analysis explored the relationship between the abundance of 15 immune cell types in the DN samples and the expression levels of the 13 EMAPRDEGs. This correlation was visualized through a dot plot (Fig. 9C). The results revealed that *ADH1B* exhibited the strongest positive correlation with memory B cells ($r = 0.79$), while *PC* showed the most significant negative correlation with natural killer cell activity ($r = -0.70$).

3.10. Verification of EMAPRDEGs expression in DN

qRT-PCR analysis was performed to measure the expression levels of the EMAPRDEGs in both DN and control blood samples. Significant differences in gene expression were observed for four genes (*CASP1*, *IL-18*, *PDK4*, and *FBP1*) with statistical significance (P

Table 4
GSEA enrichment analysis results in DN_Datasets

Description	setSize	EnrichmentScore	NES	pvalue	p.adjust	qvalue
REACTOME_ASSEMBLY_OF_COLLAGEN_FIBRILS_AND_OTHER_MULTIMERIC_STRUCTURES	47	0.64151544	2.37927903	5.467E-08	7.1588E-06	5.8347E-06
WP_INFLAMMATORY_RESPONSE_PATHWAY	26	0.67719699	2.14019254	2.2418E-05	0.00084271	0.00068684
REACTOME_MET_PROMOTES_CELL_MOTILITY	33	0.5985638	2.03937632	4.8794E-05	0.00161981	0.00132022
WP_REGULATION_OF_WNT_BCATENIN_SIGNALING_BY_SMALL_MOLECULE_COMPOUNDS	14	0.71292448	1.95151918	0.00055144	0.01192424	0.00971875

GSEA, Gene set enrichment analysis. DN, Diabetic nephropathy.

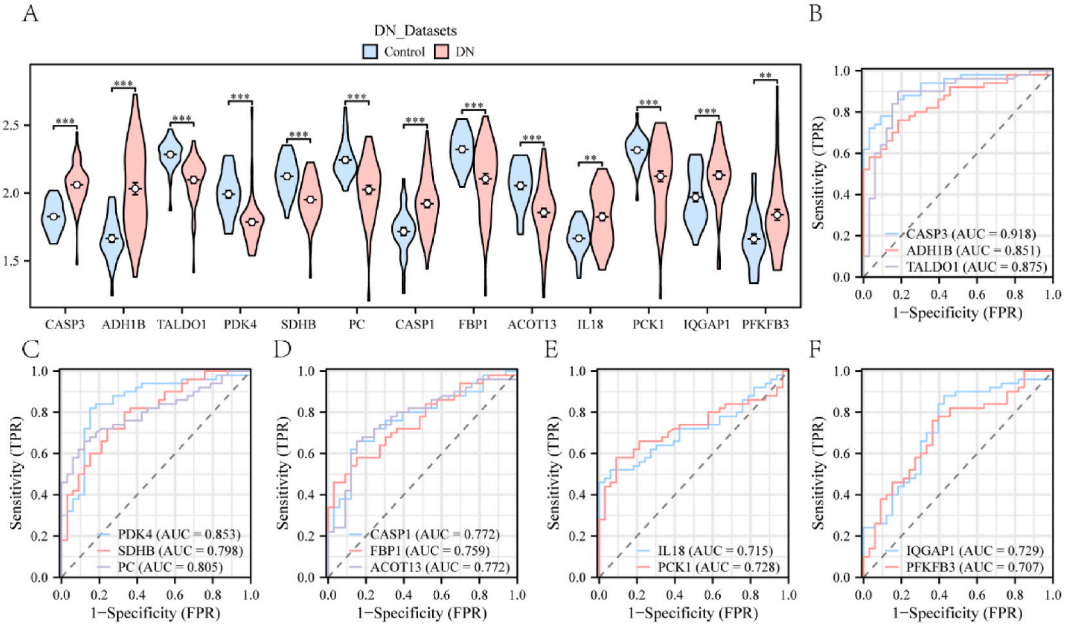

Fig. 6. Differential expression analysis and ROC analysis of EMAPRDEGs A. Group comparison plot of EMAPRDEGs in DN and Control groups in DN Datasets dataset. B-F. EMAPRDEGs: *CASP3* (B), *ADH1B* (B), *TALDO1* (B), *PDK4* (C), *SDHB* (C), *PC* (C), *CASP1* (D), *FBP1* (D), *ACOT13* (D), *IL18* (E), *PCK1* (E), *IQGAP1* (F), ROC curve of *PFKFB3* (F) between different groups (DN/Control) of DN Datasets. DN, Diabetic nephropathy. EMAPRDEGs, Energy metabolism and pyroptosis related differentially expressed genes. The symbol ** is equivalent to $P < 0.01$, which is highly statistically significant. The symbol *** is equivalent to $P < 0.001$ and highly statistically significant. The closer the AUC in the ROC curve is to 1, the better the diagnostic effect is. When AUC was 0.7–0.9, it had a certain accuracy. AUC >0.9 had high accuracy. ROC, Receiver operating characteristic curve; AUC, Area under the curve. Note: True Positive Rate (TPR) = TP/(TP + FN)TP (True Positives): The number of real cases that the model correctly predicts to be positive.FN (False Negatives): The number of false negative cases, the number of samples that the model incorrectly predicts to be negative. True Negative Rate (TNR) = TN/(TN + FP) TN (True Negatives): The number of true negative cases, the number of samples that the model correctly predicts to be negative. FP (False Positives): The number of false positive examples, the number of samples that the model incorrectly predicts to be positive.

< 0.05). Specifically, *CASP1* and *IL-18* were expressed at higher levels in the DN group compared to the control group, while *PDK4* and *FBP1* showed reduced expression in the DN group. No significant differences in expression were found for *CASP3*, *ADH1B*, *TALDO1*, *SDHB*, *PC*, *ACOT13*, *PCK1*, *IQGAP1*, and *PFKFB3* between the DN and control groups (Fig. 10).

4. Discussion

DN remains a leading cause of chronic kidney disease, posing a significant global health challenge [1]. Early detection and therapeutic interventions are urgently needed to halt its progression. Previous studies have shown that elevated glucose levels trigger oxidative stress and DNA damage, contributing to DN pathogenesis [40]. In recent years, the regulatory mechanisms underlying pyroptosis in the context of DN progression have been increasingly elucidated, with key pathways involving oxidative stress and activation of the NLRP3 inflammasome. Pyroptosis has been implicated in renal tubule fibrosis, and persistent inflammation is thought to drive renal interstitial fibrosis, ultimately impairing overall kidney function [41]. The development of DN is closely tied to disruptions in energy metabolism, and emerging evidence suggests that pyroptosis may influence these metabolic pathways [12–14]. Understanding these mechanisms could facilitate the development of novel therapeutic strategies. Consequently, identifying biomarkers associated with energy metabolism and pyroptosis is crucial for the diagnosis and treatment of DN.

Our bioinformatics analysis identified 13 key EMAPRDEGs: *CASP3*, *ADH1B*, *TALDO1*, *PDK4*, *SDHB*, *PC*, *CASP1*, *FBP1*, *ACOT13*, *IL18*, *PCK1*, *IQGAP1*, and *PFKFB3*. GO analysis revealed that these genes are predominantly involved in energy metabolism, with a particular focus on the regulation of mitochondrial function. These findings align with previous BP and MF enrichment results. KEGG pathway analysis further corroborated the involvement of these genes in critical cellular energy metabolism pathways. GSEA highlighted significant enrichment in several pathways, including collagen assembly, inflammatory response, cell migration, and Wnt/β-catenin signaling. Notably, Wnt/β-catenin signaling has been linked to renal cell injury and tubulointerstitial fibrosis in DN [42,43]. The enriched pathways associated with collagen fiber assembly underscore the role of extracellular matrix accumulation in DN progression, a finding consistent with previous research [44]. To further investigate the interactions among the identified EMAPRDEGs in DN, a PPI network was constructed, and the functional similarity of these genes was assessed. Additionally, this study explored potential miRNA and TF interactions, as well as drugs related to DN, and analyzed the expression of EMAPRDEGs in tissue-infiltrating immune cells. The diagnostic potential of these genes was also evaluated. Together, these analyses provide novel insights into the roles

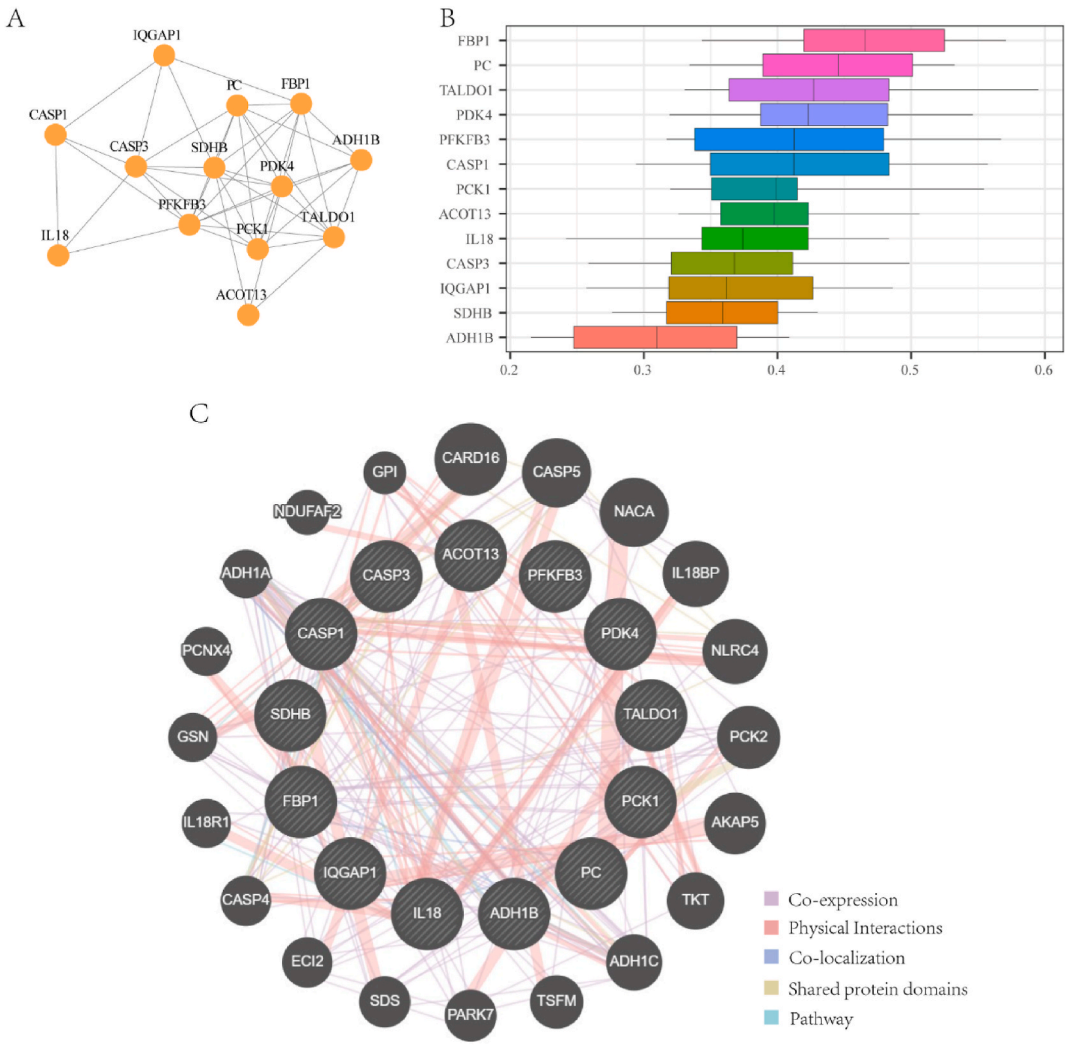

Fig. 7. PPI interaction network and functional similarity analysis A. Protein-protein interaction network (PPI network). B. Functional similarity box plot of EMAPRDEGs. C. GeneMANIA website predicted the interaction network of functionally similar genes of EMAPRDEGs. Circles in the figure show EMAPRDEGs and genes with similar functions in our study, and the corresponding colors of the lines represent the interconnected functions. PPI network, Protein-protein interaction network. EMAPRDEGs, Energy metabolism and pyroptosis related differentially expressed genes.

of energy metabolism and pyroptosis in DN pathogenesis and offer promising avenues for the development of targeted diagnostic and therapeutic strategies.

PDK4, a pivotal enzyme in the energy metabolism pathway, exhibits a broad spectrum of activities and is implicated in both physiological and pathological processes across various tissues and systems. In particular, *PDK4* regulates glucose oxidation in the myocardium [45], modulates glucagon signaling in the liver and pancreas [46], controls chronic inflammation in the skeletal muscle system [47], and contributes to endovascular calcification during advanced glycosylation [48]. Moreover, *PDK4* has been identified as a potential inhibitor of tumor growth [49]. In a high-glucose (HG) environment, downregulation of *PDK4* has been shown to protect MPC5 cells by inhibiting Vascular Endothelial Growth Factor A (VEGFA) [50]. These observations highlight a novel protective role of *PDK4* at the cellular level, emphasizing its potential as a diagnostic biomarker for chronic kidney disease [51]. Further research has revealed a strong association between PDK4 upregulation and the progression of diabetic nephropathy. In HG conditions, *PDK4* suppresses the expression of antioxidant enzymes by inhibiting the activity of nuclear factor erythroid 2-related factor 2 (Nrf2), thereby exacerbating oxidative stress [52]. These findings align with the results of the current study. Interleukin-18 (*IL-18*), a critical marker of inflammasome activation, is intricately linked to energy metabolism. Studies on *IL-18* gene knockout (*IL-18*−/−) mice have shown that IL-18 deficiency leads to a 47 % greater increase in body weight compared to wild-type mice, along with the development of hyperglycemia, hyperlipidemia, and insulin resistance with age [53]. Notably, *IL-18*−/− mice with dyslipidemia also exhibit inhibition of the Wnt signaling pathway, reduced expression of cyclin D1 (Ccnd1), and disruption of circadian rhythms [54]. *IL-18* contributes to the pathogenesis of DN through its proinflammatory effects [55], regulation of oxidative stress, and interaction with key

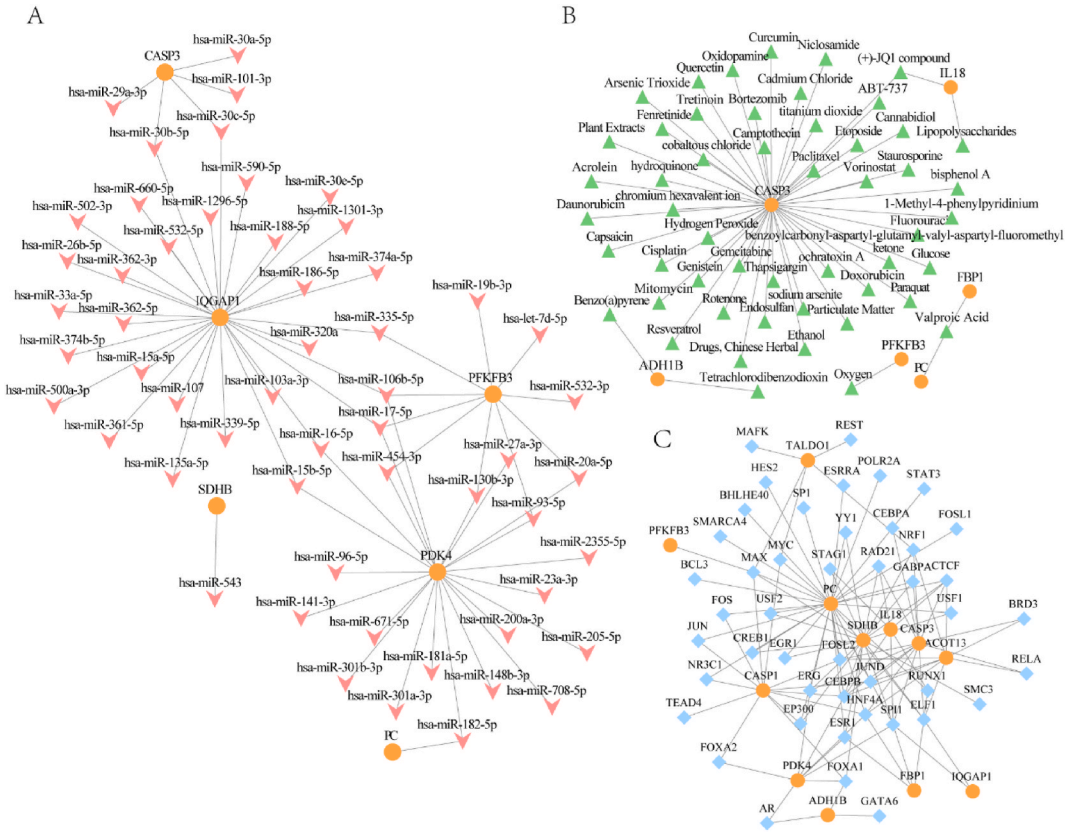

Fig. 8. Interaction network of mRNA-miRNA, mRNA-Drug and mRNA-TF A. The mRNA-miRNA interaction network diagram of EMAPRDEGs, orange circles are mRNAs and light pink V-shaped blocks are miRNAs. B. mRNA-drugs interaction network diagram of EMAPRDEGs, orange circles are mRNAs and green triangular blocks are drugs. C. mRNA-TF interaction network diagram of EMAPRDEGs, orange circles are mRNAs and blue diamonds are transcription factors (TFS). EMAPRDEGs, Energy metabolism and pyroptosis related differentially expressed genes. TF, Transcription factors.

signaling pathways [7]. Notably, elevated *IL-18* levels have been identified as a key predictor of DN onset in diabetic patients [56,57], a finding consistent with our own results, suggesting that IL-18 may serve as a reliable biomarker for DN. The development of a novel anti-IL-1R7 antibody, which mitigates *IL-18*-driven inflammation by blocking NFκB activation and reducing pro-inflammatory cytokines such as IFNγ and *IL-6* in human cells and PBMCs, further underscores the therapeutic potential of targeting *IL-18* signaling in diseases characterized by excessive *IL-18* activity, including DN [58]. *Caspase-1* (*CASP1*), a pivotal mediator of inflammation [59], is also implicated in energy metabolism [60]. Increased expression of *CASP1* in DN is associated with exacerbated inflammatory responses, a key factor in the progression of DN [6]. The identification of *CASP1* as a differentially expressed gene in our study highlights the importance of inflammation in DN pathogenesis and supports the potential of targeting inflammatory pathways as a therapeutic strategy. Fructose-1,6-bisphosphatase 1 (*FBP1*), a rate-limiting enzyme in gluconeogenesis, plays a pivotal role in regulating glucose production. In diabetes, *FBP1* upregulation has been shown to improve insulin resistance [61]. However, the precise mechanisms through which *FBP1* impacts DN and its potential therapeutic implications remain to be fully elucidated and require further investigation. *FBP1* exhibits the highest degree of functional similarity to other key genes, suggesting that it may play a comparable role in regulating energy metabolism.

miRNAs, an endogenous class of small, non-coding RNAs, are essential regulators of gene expression. Our team has successfully constructed an mRNA-miRNA network, identifying 72 miRNAs predicted to target relevant genes, some of which have been experimentally validated. For instance, hsa-miR-27a-3p has been implicated in the regulation of DN progression and is proposed as a potential therapeutic target [62]. Similarly, hsa-miR-15b-5p has been shown to protect podocytes from damage in DN [50]. Additionally, a TF-mRNA network was constructed, identifying 117 predicted target TFs. Notably, a randomized, double-blind, placebo-controlled clinical trial has demonstrated the efficacy of resveratrol in reducing albuminuria in patients with DN [63]. Furthermore, a murine study highlighted the role of quercetin in preventing mesangial cell proliferation during the early stages of DN through modulation of the Hippo signaling pathway [64], while another rat study found that curcumin alleviates DN by inhibiting inflammatory gene expression via reversal of caveolin-1Tyr(14) phosphorylation, which affects TLR4 activation [65].

The infiltration of immune cells and their correlation with the expression of EMAPRDEGs were assessed in both patients with DN and controls. Notable changes in immune cell populations were observed in DN, with ADH1B and PC exhibiting significant associations

Table 5
mRNA-miRNA interaction network nodes.

mRNA	miRNA
CASP3	hsa-miR-29a-3p
CASP3	hsa-miR-30a-5p
CASP3	hsa-miR-101-3p
CASP3	hsa-miR-30c-5p
CASP3	hsa-miR-30b-5p
IQGAP1	hsa-miR-15a-5p
IQGAP1	hsa-miR-16-5p
IQGAP1	hsa-miR-17-5p
IQGAP1	hsa-miR-26b-5p
IQGAP1	hsa-miR-33a-5p
IQGAP1	hsa-miR-103a-3p
IQGAP1	hsa-miR-107
IQGAP1	hsa-miR-30c-5p
IQGAP1	hsa-miR-15b-5p
IQGAP1	hsa-miR-30b-5p
IQGAP1	hsa-miR-135a-5p
IQGAP1	hsa-miR-186-5p
IQGAP1	hsa-miR-188-5p
IQGAP1	hsa-miR-320a
IQGAP1	hsa-miR-106b-5p
IQGAP1	hsa-miR-30e-5p
IQGAP1	hsa-miR-361-5p
IQGAP1	hsa-miR-362-5p
IQGAP1	hsa-miR-374a-5p
IQGAP1	hsa-miR-339-5p
IQGAP1	hsa-miR-335-5p
IQGAP1	hsa-miR-500a-3p
IQGAP1	hsa-miR-532-5p
IQGAP1	hsa-miR-590-5p
IQGAP1	hsa-miR-660-5p
IQGAP1	hsa-miR-362-3p
IQGAP1	hsa-miR-502-3p
IQGAP1	hsa-miR-374b-5p
IQGAP1	hsa-miR-1296-5p
IQGAP1	hsa-miR-1301-3p
PC	hsa-miR-182-5p
PDK4	hsa-miR-16-5p
PDK4	hsa-miR-17-5p
PDK4	hsa-miR-20a-5p
PDK4	hsa-miR-23a-3p
PDK4	hsa-miR-27a-3p
PDK4	hsa-miR-93-5p
PDK4	hsa-miR-96-5p
PDK4	hsa-miR-181a-5p
PDK4	hsa-miR-182-5p
PDK4	hsa-miR-205-5p
PDK4	hsa-miR-15b-5p
PDK4	hsa-miR-141-3p
PDK4	hsa-miR-106b-5p
PDK4	hsa-miR-200a-3p
PDK4	hsa-miR-301a-3p
PDK4	hsa-miR-130b-3p
PDK4	hsa-miR-148b-3p
PDK4	hsa-miR-671-5p
PDK4	hsa-miR-454-3p
PDK4	hsa-miR-708-5p
PDK4	hsa-miR-301b-3p
PDK4	hsa-miR-2355-5p
PFKFB3	hsa-let-7d-5p
PFKFB3	hsa-miR-17-5p
PFKFB3	hsa-miR-19b-3p
PFKFB3	hsa-miR-20a-5p
PFKFB3	hsa-miR-93-5p
PFKFB3	hsa-miR-106b-5p
PFKFB3	hsa-miR-130b-3p
PFKFB3	hsa-miR-335-5p
PFKFB3	hsa-miR-454-3p
PFKFB3	hsa-miR-532-3p
SDHB	hsa-miR-543

Table 6
mRNA-Drug interaction network nodes.

mRNA	Drug
ADH1B	Benzo(a)pyrene
ADH1B	Tetrachlorodibenzodioxin
CASP3	1-Methyl-4-phenylpyridinium
CASP3	ABT-737
CASP3	Acrolein
CASP3	Arsenic Trioxide
CASP3	benzoylcarbonyl-aspartyl-glutamyl-valyl-aspartyl-fluoromethyl ketone
CASP3	bisphenol A
CASP3	Bortezomib
CASP3	Cadmium Chloride
CASP3	Camptothecin
CASP3	Cannabidiol
CASP3	Capsaicin
CASP3	chromium hexavalent ion
CASP3	Cisplatin
CASP3	cobaltous chloride
CASP3	Curcumin
CASP3	Daunorubicin
CASP3	Doxorubicin
CASP3	Drugs, Chinese Herbal
CASP3	Endosulfan
CASP3	Ethanol
CASP3	Etoposide
CASP3	Fenretinide
CASP3	Fluorouracil
CASP3	Gemcitabine
CASP3	Genistein
CASP3	Glucose
CASP3	Hydrogen Peroxide
CASP3	hydroquinone
CASP3	(+)-JQ1 compound
CASP3	Mitomycin
CASP3	Niclosamide
CASP3	ochratoxin A
CASP3	Oxidopamine
CASP3	Paclitaxel
CASP3	Paraquat
CASP3	Particulate Matter
CASP3	Plant Extracts
CASP3	Quercetin
CASP3	Resveratrol
CASP3	Rotenone
CASP3	sodium arsenite
CASP3	Staurosporine
CASP3	Thapsigargin
CASP3	titanium dioxide
CASP3	Tretinoin
CASP3	Vorinostat
FBP1	Valproic Acid
IL18	(+)-JQ1 compound
IL18	Lipopolysaccharides
PC	Valproic Acid
PFKFB3	Oxygen

with natural killer (NK) cells and memory B cells. The expression level of *ADH1B* was found to correlate with various immune checkpoints, highlighting its potential role in regulating the immune microenvironment [66]. Research suggests that tissue-resident lymphocytes in the kidney are capable of rapid responses to pathogens and environmental stimuli [67]. The accumulation of these immune cells may exacerbate the inflammatory response, thereby contributing to the progression of DN. *PC*, a key regulator of cellular metabolism, particularly in cancer cells, has been linked to cellular proliferation and migration [68], suggesting that alterations in its expression could influence the immune microenvironment in DN. The immune cell correlation heatmap revealed a strong positive association between Regulatory T cells and Memory B cells, as well as a strong negative correlation between Immature dendritic cells and Immature B cells. These findings warrant further investigation to clarify underlying mechanisms. To validate the diagnostic potential of the identified genes for DN, ROC curve analysis was performed. Thirteen EMAPRDEGs demonstrated good diagnostic value for DN. qRT-PCR confirmed that the expression levels of *CASP1*, *IL-18*, *PDK4*, and *FBP1* were consistent with the bioinformatics analysis results.

While our approach builds on methodologies previously utilized [69–72], certain limitations remain. First, the sample size may

Table 7
mRNA-TF interaction network nodes.

mRNA	TF
CASP3	CTCF
CASP3	ELF1
CASP3	FOSL2
CASP3	HNF4A
CASP3	JUND
CASP3	NRF1
CASP3	BRD3
CASP3	RELA
CASP3	CEBPB
ACOT13	CTCF
ACOT13	ELF1
ACOT13	FOSL2
ACOT13	HNF4A
ACOT13	JUND
ACOT13	NRF1
ACOT13	BRD3
ACOT13	RELA
ACOT13	CEBPB
ADH1B	AR
ADH1B	FOXA1
ADH1B	GATA6
CASP1	CEBPB
CASP1	EP300
CASP1	FOS
CASP1	FOSL2
CASP1	FOXA1
CASP1	FOXA2
CASP1	HNF4A
CASP1	JUN
CASP1	JUND
CASP1	MAX
CASP1	MYC
CASP1	NR3C1
CASP1	TEAD4
CASP3	CEBPA
CASP3	ERG
CASP3	GABPA
CASP3	RAD21
CASP3	SPI1
FBP1	HNF4A
FBP1	RUNX1
FBP1	SPI1
FBP1	ESR1
IL18	RAD21
IL18	RUNX1
IL18	SPI1
IL18	STAG1
IL18	CEBPB
IL18	CTCF
IQGAP1	ELF1
IQGAP1	SPI1
PC	BCL3
PC	BHLHE40
PC	CEBPA
PC	CEBPB
PC	CREB1
PC	CTCF
PC	EGR1
PC	ELF1
PC	EP300
PC	ERG
PC	ESR1
PC	ESRRA
PC	FOS
PC	FOSL1
PC	FOSL2
PC	GABPA
PC	HES2

(*continued on next page*)

Table 7 (*continued*)

mRNA	TF
PC	HNF4A
PC	JUN
PC	JUND
PC	MAX
PC	MYC
PC	NR3C1
PC	POLR2A
PC	RAD21
PC	RUNX1
PC	SMARCA4
PC	SP1
PC	SPI1
PC	STAT3
PC	USF1
PC	USF2
PC	YY1
PDK4	AR
PDK4	CEBPB
PDK4	ERG
PDK4	ESR1
PDK4	FOXA1
PDK4	FOXA2
PDK4	HNF4A
PDK4	SPI1
PFKFB3	MAX
SDHB	CEBPB
SDHB	CREB1
SDHB	CTCF
SDHB	EGR1
SDHB	ELF1
SDHB	EP300
SDHB	ERG
SDHB	ESR1
SDHB	FOXA1
SDHB	GABPA
SDHB	MAX
SDHB	NRF1
SDHB	RAD21
SDHB	SMC3
SDHB	SPI1
SDHB	STAG1
SDHB	USF1
SDHB	USF2
SDHB	YY1
TALDO1	MAFK
TALDO1	MAX
TALDO1	MYC
TALDO1	NRF1
TALDO1	REST

TF; Transcription factors.

have compromised the robustness of our findings, as evidenced by qRT-PCR validation. Future studies should aim to increase the sample size to enhance the reliability of the results. Second, although the FDR method was applied to minimize false positives and improve result confidence, the study design still poses risks of multiple comparison biases, which must be rigorously controlled to ensure result reliability. Third, as our study relies on GEO data, potential biases related to sample selection, data diversity, quality, and consistency must be considered. To address these issues in future experimental verification, integrating multiple data sources, expanding the sample size and diversity, and ensuring data quality will be critical. Additionally, the prognostic value of the identified EMAPRDEGs remains uncertain. This study marks the first effort to link genes involved in energy metabolism and pyroptosis in DN, suggesting that these genes may play significant roles in the pathogenesis and progression of the disease. However, further validation is necessary to substantiate these findings.

5. Conclusions

Bioinformatics analysis identified 13 EMAPRDEGs potentially associated with DN. Among these, *CASP1*, *IL-18*, *PDK4*, and *FBP1* emerged as promising biological markers for DN, warranting further validation. *CASP1* is linked to an enhanced inflammatory response in DN, with its expression level potentially serving as an indicator of inflammation severity. *IL-18*, a key regulator of both

Table 8
Primer sequences for quantitative real-time PCR.

Gene Names	Forward (5′-3′)	Reverse (3'-5')
CASP3	TGTTTGTGTGCTTCTGAGCC	CACGCCATGTCATCATCAAC
ADH1B	TGCTGAACCAAACTGTGCTG	TGCAACATTGGCTAAGTCGG
TALDO1	CAGCACAGATGCCCGCTTA	CGGCCCGGAATCTTCTTTAGTA
PDK4	GGAGCATTTCTCGCGCTACA	ACAGGCAATTCTTGTCGCAAA
SDHB	AAGCATCCAATACCATGGGG	TCTATCGATGGGACCCAGAC
PC	GGCTACACCTACCCAGAC	GGAGTCAAACACACGGAAGAC
CASP1	GAGCTTCAGTCAGGTCCATCA	TCTGAGGTCAACATCAGCTCC
FBP1	AGCAGTCAAAGCCATCTCTTC	ACGTCCAGCTTCTTAACTTGA
ACOT13	AGCAGCATGACCCAGAACCTA	GGAGCGTGCCCAGTTTATTAGTA
IL18	GACTGGCTGTGACCCTATCT	TTCCATTTTGTTGTGTCCTG
PCK1	AGCATTCAACGCCAGGTTC	CGAGTCTGTCAGTTCAATACCAA
IQGAP1	TTCTATGCAGCTTTCTCGGG	CTGTCGAACTAAGTATCCACGG
PFKFB3	GATGCCCTTCAGGAAAGCCT	TCCCCGACGTTGAACACTTT
ACTIN	AGCCTTCCTTCCTGGGCAT	TGATCTTCATTGTGCTGGGTG

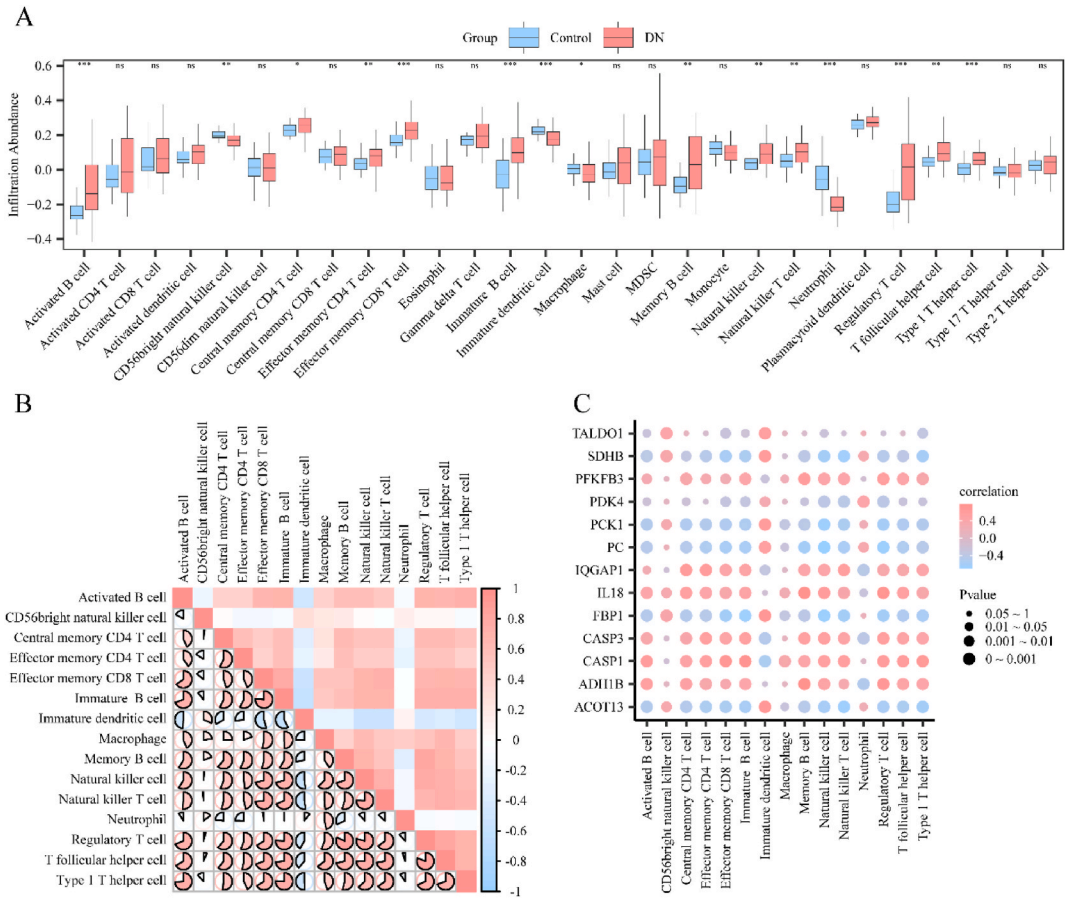

Fig. 9. Immune Infiltration Analysis of DN Datasets (ssGSEA) A. Box plot of grouping comparison of immune cells under DN and Control groups in the DN Datasets dataset. B. Heat map of correlations between the 15 immune cells with significant differences in DN Datasets dataset. C. Dot plot of correlation between EMAPRDEGs expression and infiltration abundance of 15 immune cells in DN Datasets dataset. The symbol ns was equivalent to $P \geq 0.05$, which was not statistically significant. The symbol * is equivalent to $P < 0.05$, which is statistically significant; The symbol ** is equivalent to $P < 0.01$, which is highly statistically significant; The symbol *** is equivalent to $P < 0.001$ and highly statistically significant. DN, Diabetic nephropathy. EMAPRDEGs, Energy metabolism and pyroptosis related differentially expressed genes. ssGSEA, single-sample gene-set enrichment analysis. The absolute value of correlation coefficient (r value) below 0.3 was weak or no correlation, 0.3–0.5 was weak correlation, 0.5–0.8 was moderate correlation, and above 0.8 was strong correlation. The light blue is the Control group, and the light red is the diabetic nephropathy (DN) group. In the correlation heat map, red is positive correlation, blue is negative correlation, and the depth of color represents the strength of correlation.

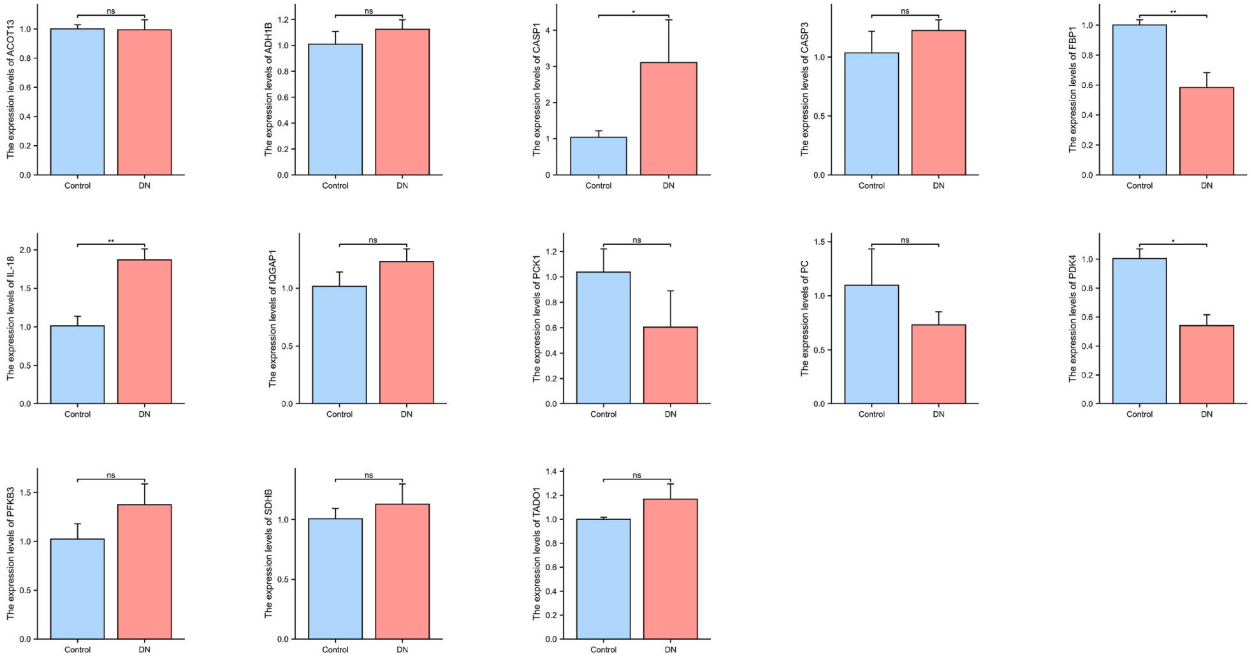

Fig. 10. Validation of the differential expression of potential diagnostic markers *PC, SDHB, ADH1B, ACOT13, PDK4, CASP1, IQGAP1, TALDO1, PCK1, PFKFB3, FBP1, CASP3* and *IL18* via qRT-PCR. *P < 0.05, **P < 0.01; ns: not significant.

inflammation and energy metabolism, has rising levels that are considered a key predictor of DN progression.

CRediT authorship contribution statement

Shan He: Writing – original draft, Methodology, Data curation. **Jian Ye:** Writing – original draft, Data curation. **Yu Wang:** Funding acquisition. **Lu yang Xie:** Software. **Si Yi Liu:** Supervision. **Qin kai Chen:** Writing – review & editing, Supervision, Methodology.

Ethics approval and consent to participate and publication

This study was reviewed and approved by the Ethics Committee of the First Affiliated Hospital of Nanchang University, with the approval number: (2024) CDYFYYLK (07–026), dated July 22, 2024. All participants provided written informed consent to participate in the study and for their data to be published. This study was conducted in accordance with the ethical principles outlined in the Declaration of Helsinki, as established by the World Medical Association.

Data availability statement

Data are available on reasonable request. All data relevant to the study are included in the article or uploaded as supplemental information. Gene expression data from the GEO repository (https://www.ncbi.nlm.nih.gov/geo/) include the following datasets: GSE30528, GSE96804.

Funding

This study was supported by the Fund of Jiangxi Provincial Natural Science Foundation (Grant number: 20212BAB206028, 20232BAB206034).

Declaration of competing interest

The authors declare that they have no known competing financial interests or personal relationships that could have appeared to influence the work reported in this paper.

Acknowledgements

Not applicable.

References

[1] K. Umanath, J.B. Lewis, Update on diabetic nephropathy: core curriculum 2018, Am. J. Kidney Dis. 71 (6) (2018) 884–895, https://doi.org/10.1053/j.ajkd.2017.10.026.

[2] V. Perkovic, M.J. Jardine, B. Neal, S. Bompoint, H.J.L. Heerspink, D.M. Charytan, R. Edwards, R. Agarwal, G. Bakris, et al., Canagliflozin and renal outcomes in type 2 diabetes and nephropathy, N. Engl. J. Med. 380 (24) (2019) 2295–2306, https://doi.org/10.1056/NEJMoa1811744.

[3] X. Liu, H. Du, Y. Sun, L. Shao, Role of abnormal energy metabolism in the progression of chronic kidney disease and drug intervention, Ren. Fail. 44 (1) (2022) 790–805, https://doi.org/10.1080/0886022X.2022.2072743.

[4] T. Imasawa, E. Obre, N. Bellance, J. Lavie, T. Imasawa, C. Rigothier, Y. Delmas, C. Combe, D. Lacombe, et al., High glucose repatterns human podocyte energy metabolism during differentiation and diabetic nephropathy, FASEB J 31 (1) (2017) 294–307, https://doi.org/10.1096/fj.201600293R.

[5] L. Thongnak, A. Pongchaidecha, A. Lungkaphin, Renal lipid metabolism and lipotoxicity in diabetes, Am. J. Med. Sci. 359 (2) (2020) 84–99, https://doi.org/10.1016/j.amjms.2019.11.004.

[6] Y. Zuo, L. Chen, H. Gu, X. He, Z. Ye, Z. Wang, Q. Shao, C. Xue, GSDMD-mediated pyroptosis: a critical mechanism of diabetic nephropathy, Expert Rev Mol Med 23 (2021) e23, https://doi.org/10.1017/erm.2021.27.

[7] X. Liu, J. Lieberman, A mechanistic understanding of pyroptosis: the fiery death triggered by invasive infection, Adv. Immunol. 135 (2017), https://doi.org/10.1016/bs.ai.2017.02.002.

[8] Y. Zhang, X. Chen, C. Gueydan, J. Han, Plasma membrane changes during programmed cell deaths, Cell Res. 28 (1) (2018), https://doi.org/10.1038/cr.2017.133.

[9] Y. Wang, T.-D. Kanneganti, From pyroptosis, apoptosis and necroptosis to PANoptosis: a mechanistic compendium of programmed cell death pathways, Comput. Struct. Biotechnol. J. 19 (2021) 4641–4657, https://doi.org/10.1016/j.csbj.2021.07.038.

[10] S. Fougeray, I. Mami, G. Bertho, P. Beaune, E. Thervet, N. Pallet, Tryptophan depletion and the kinase GCN2 mediate IFN-γ-induced autophagy, J. Immunol. 189 (6) (2012) 2954–2964, https://doi.org/10.4049/jimmunol.1201214.

[11] J. Wu, S. Rong, J. Zhou, W. Yuan, The role and mechanism of PKM2 in the development of LPS-induced acute kidney injury, Histol. Histopathol. 36 (8) (2021) 845–852, https://doi.org/10.14670/HH-18-343.

[12] L. Zhao, Y. Hao, S. Tang, X. Han, R. Li, X. Zhou, Energy metabolic reprogramming regulates programmed cell death of renal tubular epithelial cells and might serve as a new therapeutic target for acute kidney injury, Front. Cell Dev. Biol. 11 (2023) 1276217, https://doi.org/10.3389/fcell.2023.1276217.

[13] H. Li, D.-H. Yang, Y. Zhang, F. Zheng, F. Gao, J. Sun, G. Shi, Geniposide suppresses NLRP3 inflammasome-mediated pyroptosis via the AMPK signaling pathway to mitigate myocardial ischemia/reperfusion injury, Chin. Med. 17 (1) (2022) 73, https://doi.org/10.1186/s13020-022-00616-5.

[14] P. Su, X. Mao, J. Ma, L. Huang, L. Yu, S. Tang, M. Zhuang, Z. Lu, K.S. Osafo, et al., ERRα promotes glycolytic metabolism and targets the NLRP3/caspase-1/GSDMD pathway to regulate pyroptosis in endometrial cancer, J. Exp. Clin. Cancer Res. 42 (1) (2023) 274, https://doi.org/10.1186/s13046-023-02834-7.

[15] J. Hao, Q. Wei, S. Mei, L. Li, Y. Su, C. Mei, Z. Dong, Induction of microRNA-17-5p by p53 protects against renal ischemia-reperfusion injury by targeting death receptor 6, Kidney Int. 91 (1) (2017) 106–118, https://doi.org/10.1016/j.kint.2016.07.017.

[16] S. Davis, P.S. Meltzer, GEOquery: a bridge between the gene expression Omnibus (GEO) and BioConductor, Bioinformatics 23 (14) (2007) 1846–1847.

[17] K.I. Woroniecka, A.S. Park, D. Mohtat, D.B. Thomas, J.M. Pullman, K. Susztak, Transcriptome analysis of human diabetic kidney disease, Diabetes 60 (9) (2011) 2354–2369, https://doi.org/10.2337/db10-1181.

[18] Y. Pan, S. Jiang, Q. Hou, D. Qiu, J. Shi, L. Wang, Z. Chen, M. Zhang, A. Duan, et al., Dissection of glomerular transcriptional profile in patients with diabetic nephropathy: SRGAP2a protects podocyte structure and function, Diabetes 67 (4) (2018) 717–730, https://doi.org/10.2337/db17-0755.

[19] J.-S. Shi, D.-D. Qiu, W.-B. Le, H. Wang, S. Li, Y.-H. Lu, S. Jiang, Identification of transcription regulatory relationships in diabetic nephropathy, Chinese Med J 131 (23) (2018) 2886–2890, https://doi.org/10.4103/0366-6999.246063.

[20] J.T. Leek, W.E. Johnson, H.S. Parker, A.E. Jaffe, J.D. Storey, The sva package for removing batch effects and other unwanted variation in high-throughput experiments, Bioinformatics 28 (6) (2012) 882–883, https://doi.org/10.1093/bioinformatics/bts034.

[21] G. Stelzer, N. Rosen, I. Plaschkes, S. Zimmerman, M. Twik, S. Fishilevich, T.I. Stein, R. Nudel, I. Lieder, et al., The GeneCards suite: from gene data mining to disease genome sequence analyses, Curr Protoc Bioinformatics 54 (2016), https://doi.org/10.1002/cpbi.5.

[22] H. Chen, R. Jiang, W. Huang, K. Chen, R. Zeng, H. Wu, Q. Yang, K. Guo, J. Li, et al., Identification of energy metabolism-related biomarkers for risk prediction of heart failure patients using random forest algorithm, Front. Cardiovasc. Med. 9 (2022) 993142, https://doi.org/10.3389/fcvm.2022.993142.

[23] Q. Chen, F. Li, Y. Gao, G. Xu, L. Liang, J. Xu, Identification of energy metabolism genes for the prediction of survival in hepatocellular carcinoma, Front. Oncol. 10 (2020) 1210, https://doi.org/10.3389/fonc.2020.01210.

[24] H. Liu, J. Zhang, C. Wei, Z. Liu, W. Zhou, P. Yang, Y. Gong, Y. Zhao, Prognostic signature construction of energy metabolism-related genes in pancreatic cancer, Front. Oncol. 12 (2022) 917897, https://doi.org/10.3389/fonc.2022.917897.

[25] T. Mu, H. Li, X. Li, Prognostic implication of energy metabolism-related gene signatures in lung adenocarcinoma, Front. Oncol. 12 (2022) 867470, https://doi.org/10.3389/fonc.2022.867470.

[26] Z. Dong, L. Bian, M. Wang, L. Wang, Y. Wang, Identification of a pyroptosis-related gene signature for prediction of overall survival in lung adenocarcinoma, J Oncol 2021 (2021) 6365459, https://doi.org/10.1155/2021/6365459.

[27] Gene ontology consortium: going forward, Nucleic Acids Res. 43 (Database issue) (2015) D1049–D1056, https://doi.org/10.1093/nar/gku1179.

[28] M. Kanehisa, S. Goto, KEGG: kyoto encyclopedia of genes and genomes, Nucleic Acids Res. 28 (1) (2000) 27–30.

[29] G. Yu, L.-G. Wang, Y. Han, Q.-Y. He, clusterProfiler: an R package for comparing biological themes among gene clusters, OMICS 16 (5) (2012) 284–287, https://doi.org/10.1089/omi.2011.0118.

[30] A. Subramanian, P. Tamayo, V.K. Mootha, S. Mukherjee, B.L. Ebert, M.A. Gillette, A. Paulovich, S.L. Pomeroy, T.R. Golub, et al., Gene set enrichment analysis: a knowledge-based approach for interpreting genome-wide expression profiles, Proc Natl Acad Sci U S A 102 (43) (2005) 15545–15550.

[31] A. Liberzon, C. Birger, H. Thorvaldsdóttir, M. Ghandi, J.P. Mesirov, P. Tamayo, The Molecular Signatures Database (MSigDB) hallmark gene set collection, Cell Syst 1 (6) (2015) 417–425.

[32] S.H. Park, J.M. Goo, C.-H. Jo, Receiver operating characteristic (ROC) curve: practical review for radiologists, Korean J. Radiol. 5 (1) (2004) 11–18.

[33] D. Szklarczyk, A.L. Gable, D. Lyon, A. Junge, S. Wyder, J. Huerta-Cepas, M. Simonovic, N.T. Doncheva, J.H. Morris, et al., STRING v11: protein-protein association networks with increased coverage, supporting functional discovery in genome-wide experimental datasets, Nucleic Acids Res. 47 (D1) (2019) D607–D613, https://doi.org/10.1093/nar/gky1131.

[34] P. Shannon, A. Markiel, O. Ozier, N.S. Baliga, J.T. Wang, D. Ramage, N. Amin, B. Schwikowski, T. Ideker, Cytoscape: a software environment for integrated models of biomolecular interaction networks, Genome Res. 13 (11) (2003) 2498–2504.

[35] G. Yu, F. Li, Y. Qin, X. Bo, Y. Wu, S. Wang, GOSemSim: an R package for measuring semantic similarity among GO terms and gene products, Bioinformatics 26 (7) (2010) 976–978, https://doi.org/10.1093/bioinformatics/btq064.

[36] M. Franz, H. Rodriguez, C. Lopes, K. Zuberi, J. Montojo, G.D. Bader, Q. Morris, GeneMANIA update 2018, Nucleic Acids Res. 46 (W1) (2018) W60–W64, https://doi.org/10.1093/nar/gky311.

[37] K.-R. Zhou, S. Liu, W.-J. Sun, L.-L. Zheng, H. Zhou, J.-H. Yang, L.-H. Qu, ChIPBase v2.0: decoding transcriptional regulatory networks of non-coding RNAs and protein-coding genes from ChIP-seq data, Nucleic Acids Res. 45 (D1) (2017) D43–D50, https://doi.org/10.1093/nar/gkw965.

[38] A.P. Davis, C.J. Grondin, R.J. Johnson, D. Sciaky, J. Wiegers, T.C. Wiegers, C.J. Mattingly, Comparative Toxicogenomics database (CTD): update 2021, Nucleic Acids Res. 49 (D1) (2021) D1138–D1143, https://doi.org/10.1093/nar/gkaa891.

[39] B. Xiao, L. Liu, A. Li, C. Xiang, P. Wang, H. Li, T. Xiao, Identification and verification of immune-related gene prognostic signature based on ssGSEA for osteosarcoma, Front. Oncol. 10 (2020) 607622, https://doi.org/10.3389/fonc.2020.607622.

[40] R. Vishakh, N. Suchetha Kumari, A. Bhandary, S.S. Shetty, P. Bhandary, Selvan G. Tamizh, Evaluating the role of cytokinesis-block micronucleus assay as a biomarker for oxidative stress-inducing DNA damage in type 2 diabetes mellitus patients, Beni-Suef University Journal of Basic and Applied Sciences 12 (1) (2023) 56, https://doi.org/10.1186/s43088-023-00384-7.

[41] Z. Zhou, Q. Li, The role of pyroptosis in the pathogenesis of kidney diseases, Kidney Dis. 9 (6) (2023) 443–458, https://doi.org/10.1159/000531642.

[42] C. Dai, D.B. Stolz, L.P. Kiss, S.P. Monga, L.B. Holzman, Y. Liu, Wnt/beta-catenin signaling promotes podocyte dysfunction and albuminuria, J. Am. Soc. Nephrol. 20 (9) (2009) 1997–2008, https://doi.org/10.1681/ASN.2009010019.

[43] T. Zhou, X. He, R. Cheng, B. Zhang, R.R. Zhang, Y. Chen, Y. Takahashi, A.R. Murray, K. Lee, et al., Implication of dysregulation of the canonical wingless-type MMTV integration site (WNT) pathway in diabetic nephropathy, Diabetologia 55 (1) (2012) 255–266, https://doi.org/10.1007/s00125-011-2314-2.

[44] R.M. Mason, N.A. Wahab, Extracellular matrix metabolism in diabetic nephropathy, J. Am. Soc. Nephrol. 14 (5) (2003) 1358–1373.

[45] B.-Y. Park, J.-H. Jeon, Y. Go, H.J. Ham, J.-E. Kim, E.K. Yoo, W.H. Kwon, N.-H. Jeoung, Y.H. Jeon, et al., PDK4 deficiency suppresses hepatic glucagon signaling by decreasing cAMP levels, Diabetes 67 (10) (2018) 2054–2068, https://doi.org/10.2337/db17-1529.

[46] L. Janah, S. Kjeldsen, K.D. Galsgaard, M. Winther-Sørensen, E. Stojanovska, J. Pedersen, F.K. Knop, J.J. Holst, N.J. Wewer Albrechtsen, Glucagon receptor signaling and glucagon resistance, Int. J. Mol. Sci. 20 (13) (2019), https://doi.org/10.3390/ijms20133314.

[47] H. Park, N.H. Jeoung, Inflammation increases pyruvate dehydrogenase kinase 4 (PDK4) expression via the Jun N-Terminal Kinase (JNK) pathway in C2C12 cells, Biochem. Biophys. Res. Commun. 469 (4) (2016) 1049–1054, https://doi.org/10.1016/j.bbrc.2015.12.113.

[48] J. Leem, I.K. Lee, Mechanisms of vascular calcification: the pivotal role of pyruvate dehydrogenase kinase 4, Endocrinol Metab (Seoul) 31 (1) (2016) 52–61, https://doi.org/10.3803/EnM.2016.31.1.52.

[49] D. Leclerc, N. Lévesque, Y. Cao, L. Deng, Q. Wu, J. Powell, C. Sapienza, R. Rozen, Genes with aberrant expression in murine preneoplastic intestine show epigenetic and expression changes in normal mucosa of colon cancer patients, Cancer Prev. Res. 6 (11) (2013) 1171–1181, https://doi.org/10.1158/1940-6207.CAPR-13-0198.

[50] T. Zhao, Q. Jin, L. Kong, D. Zhang, Y. Teng, L. Lin, X. Yao, Y. Jin, M. Li, microRNA-15b-5p shuttled by mesenchymal stem cell-derived extracellular vesicles protects podocytes from diabetic nephropathy via downregulation of VEGF/PDK4 axis, J. Bioenerg. Biomembr. 54 (1) (2022) 17–30, https://doi.org/10.1007/s10863-021-09919-y.

[51] Y. Zhou, Z. Yu, L. Liu, L. Wei, L. Zhao, L. Huang, L. Wang, S. Sun, Construction and evaluation of an integrated predictive model for chronic kidney disease based on the random forest and artificial neural network approaches, Biochem. Biophys. Res. Commun. 603 (2022) 21–28, https://doi.org/10.1016/j.bbrc.2022.02.099.

[52] S. Tian, X. Yang, Y. Lin, X. Li, S. Zhou, P. Yu, Y. Zhao, PDK4-mediated Nrf2 inactivation contributes to oxidative stress and diabetic kidney injury, Cell. Signal. 121 (2024) 111282, https://doi.org/10.1016/j.cellsig.2024.111282.

[53] M.G. Netea, L.A.B. Joosten, E. Lewis, D.R. Jensen, P.J. Voshol, B.J. Kullberg, C.J. Tack, H. van Krieken, S.-H. Kim, et al., Deficiency of interleukin-18 in mice leads to hyperphagia, obesity and insulin resistance, Nat Med 12 (6) (2006) 650–656.

[54] K. Yamanishi, S. Maeda, S. Kuwahara-Otani, Y. Watanabe, M. Yoshida, K. Ikubo, D. Okuzaki, Y. El-Darawish, W. Li, et al., Interleukin-18-deficient mice develop dyslipidemia resulting in nonalcoholic fatty liver disease and steatohepatitis, Transl. Res. 173 (2016), https://doi.org/10.1016/j.trsl.2016.03.010.

[55] R. Gui, Y. Ren, Z. Wang, Y. Li, C. Wu, X. Li, M. Li, Y. Li, L. Qian, et al., Deciphering interleukin-18 in diabetes and its complications: biological features, mechanisms, and therapeutic perspectives, Obes. Rev. 25 (11) (2024) e13818, https://doi.org/10.1111/obr.13818.

[56] H. Yaribeygi, M.T. Mohammadi, R. Rezaee, A. Sahebkar, Crocin improves renal function by declining Nox-4, IL-18, and p53 expression levels in an experimental model of diabetic nephropathy, J. Cell. Biochem. 119 (7) (2018) 6080–6093, https://doi.org/10.1002/jcb.26806.

[57] K. Miyauchi, Y. Takiyama, J. Honjyo, M. Tateno, M. Haneda, Upregulated IL-18 expression in type 2 diabetic subjects with nephropathy: TGF-beta1 enhanced IL-18 expression in human renal proximal tubular epithelial cells, Diabetes Res. Clin. Pract. 83 (2) (2009) 190–199, https://doi.org/10.1016/j.diabres.2008.11.018.

[58] S. Li, L. Jiang, K. Beckmann, J.F. Højen, U. Pessara, N.E. Powers, D.M. de Graaf, T. Azam, J. Lindenberger, et al., A novel anti-human IL-1R7 antibody reduces IL-18-mediated inflammatory signaling, J. Biol. Chem. 296 (2021) 100630, https://doi.org/10.1016/j.jbc.2021.100630.

[59] W. Shao, G. Yeretssian, K. Doiron, S.N. Hussain, M. Saleh, The caspase-1 digestome identifies the glycolysis pathway as a target during infection and septic shock, J. Biol. Chem. 282 (50) (2007) 36321–36329.

[60] F. Martinon, J. Tschopp, Inflammatory caspases: linking an intracellular innate immune system to autoinflammatory diseases, Cell 117 (5) (2004) 561–574.

[61] P. Li, K. Li, W. Yuan, Y. Xu, P. Li, R. Wu, J. Han, Z. Yin, L. Lu, et al., 1α,25(OH)2D3 ameliorates insulin resistance by alleviating γδ T cell inflammation via enhancing fructose-1,6-bisphosphatase 1 expression, Theranostics 13 (15) (2023) 5290–5304, https://doi.org/10.7150/thno.84645.

[62] L. Wu, Q. Wang, F. Guo, X. Ma, J. Wang, Y. Zhao, Y. Yan, G. Qin, Involvement of miR-27a-3p in diabetic nephropathy via affecting renal fibrosis, mitochondrial dysfunction, and endoplasmic reticulum stress, J. Cell. Physiol. 236 (2) (2021) 1454–1468, https://doi.org/10.1002/jcp.29951.

[63] A. Sattarinezhad, J. Roozbeh, B. Shirazi Yeganeh, G.R. Omrani, M. Shams, Resveratrol reduces albuminuria in diabetic nephropathy: a randomized double-blind placebo-controlled clinical trial, Diabetes Metab. 45 (1) (2019) 53–59, https://doi.org/10.1016/j.diabet.2018.05.010.

[64] D. Lei, L. Chengcheng, Q. Xuan, C. Yibing, W. Lei, Y. Hao, L. Xizhi, L. Yuan, Y. Xiaoxing, et al., Quercetin inhibited mesangial cell proliferation of early diabetic nephropathy through the Hippo pathway, Pharmacol. Res. 146 (2019) 104320, https://doi.org/10.1016/j.phrs.2019.104320.

[65] L.-N. Sun, Z.-Y. Yang, S.-S. Lv, X.-C. Liu, G.-J. Guan, G. Liu, Curcumin prevents diabetic nephropathy against inflammatory response via reversing caveolin-1 Tyr14 phosphorylation influenced TLR4 activation, Int Immunopharmacol 23 (1) (2014) 236–246, https://doi.org/10.1016/j.intimp.2014.08.023.

[66] Z. Xu, B. Peng, F. Kang, W. Zhang, M. Xiao, J. Li, Q. Hong, Y. Cai, W. Liu, et al., The roles of drug metabolism-related ADH1B in immune regulation and therapeutic response of ovarian cancer, Front. Cell Dev. Biol. 10 (2022) 877254, https://doi.org/10.3389/fcell.2022.877254.

[67] M. Becker, A.-C. Gnirck, J.-E. Turner, Innate lymphoid cells in renal inflammation, Front. Immunol. 11 (2020) 72, https://doi.org/10.3389/fimmu.2020.00072.

[68] A. Strickaert, C. Corbet, S.-A. Spinette, L. Craciun, G. Dom, G. Andry, D. Larsimont, R. Wattiez, J.E. Dumont, et al., Reprogramming of energy metabolism: increased expression and roles of pyruvate Carboxylase in papillary thyroid cancer, Thyroid 29 (6) (2019) 845–857, https://doi.org/10.1089/thy.2018.0435.

[69] L. Ou, H. Liu, C. Peng, Y. Zou, J. Jia, H. Li, Z. Feng, G. Zhang, M. Yao, Helicobacter pylori infection facilitates cell migration and potentially impact clinical outcomes in gastric cancer, Heliyon 10 (17) (2024) e37046, https://doi.org/10.1016/j.heliyon.2024.e37046.

[70] Y. Wang, J. Wang, T. Zeng, J. Qi, Data-mining-based biomarker evaluation and experimental validation of SHTN1 for bladder cancer, Cancer Genet 288–289 (2024) 43–53, https://doi.org/10.1016/j.cancergen.2024.09.002.

[71] G.T. Selvan, P. Gollapalli, P. Shetty, N.S. Kumari, Exploring key molecular signatures of immune responses and pathways associated with tuberculosis in comorbid diabetes mellitus: a systems biology approach, Beni-Suef University Journal of Basic and Applied Sciences 11 (1) (2022) 77, https://doi.org/10.1186/s43088-022-00257-5.

[72] P. Gollapalli, N.S. Kumari, P. Shetty, T.S. Gnanasekaran, Molecular basis of AR and STK11 genes associated pathogenesis via AMPK pathway and adipocytokine signalling pathway in the development of metabolic disorders in PCOS women, Beni-Suef University Journal of Basic and Applied Sciences 11 (1) (2022) 23, https://doi.org/10.1186/s43088-022-00200-8.